Comparison of Kurucz Model Flux Distribution with Observed Spectra

INTERNSHIP PROJECT REPORT

by

Kiran, L. `SC17B150`

Department of Earth and Space Science

Indian Institute of Space Science and Technology

Thiruvananthapuram

September, 2020

BONAFIDE CERTIFICATE

This is to certify that this project report entitled **"Synthetic Spectrum Fitting With Kurucz Models"** submitted to **Indian Institute of Space Science and Technology, Thriruvananthapuram**, is a bonafide record of work done by **"Kiran, L."** under my supervision from **"6 July 2020"** to **"14 August 2020"**.

Dr. Sarita Vig
Department of Earth and Space Science

Dr. Samir Mandal
Head of Department
Department of Earth and Space Science

Place: Thiruvananthapuram
Date: September 1, 2020

Declaration

This is to declare that this report has been written by me. No part of the report is plagiarized from other sources. All information included from other sources have been duly acknowledged. I aver that if any part of the report is found to be plagiarized, I shall take full responsibility for it.

Kiran, L.
SC17B150

Place: Thiruvananthapuram
Date: September 1, 2020

Abstract

Stellar atmosphere modelling is an important step in the synthetic spectrum method of determining physical and chemcial properties of any stellar source. With other methods for determination of the same being more laborious, synthetic spectrum fitting method has gained popularity. The aim of the present project is to analyse Kurucz models (Castelli and Kurucz, 2004) generated from ATLAS9 by comparing the model flux distribution with that observed for real stars. The model flux distribution for Kurucz models with parameters in between the grid are obtained using Python's PySynphot library. Analysis is performed on two different datasets - STELIB (optical data) and NASA IRTF (infrared data). Main sequence stars, subgiants, giants, and horizontal branch stars are included in the analysis We observe good match between Kurucz model flux distribution with observed flux distribution for main sequence stars in both optical and infrared wavelength ranges. Horizontal branch stars are found to be well fit by Kurucz models, with no model available for hypergiant stars. Despite good fit in flux distribution, significant mismatch in photometric magnitude values is observed in horizontal branch stars. Best fit in flux distribution and best match in apparent magnitudes is observed for main sequence stars, with goodness of fit decreasing for subgiant and giant stars.

Keywords: Kurucz Models, PySynphot, main sequence stars, horizontal branch stars, subgiants, giants, hypergiants, STELIB, IRTF.

Acknowledgements

I take this opportunity to express our profound gratitude and deep regards to my internship guide Dr. Sarita Vig, Associate Professor, Department of Earth and Space Science, for her exemplary guidance, monitoring and constant encouragement throughout the course of this project. The blessing, help and guidance given by her, time to time shall carry me a long way in the journey of life on which I am about to embark.

I thank my beloved parents, siblings and dear friends for their continued support and encouragement for the successful completion of our project. The valuable discussions held with Bhavana Dinesh, M.S in Astronomy and Astrophysics, IIST was very helpful in completion of this internship project. Hence, I would like to express my heartfelt gratitude to her.

Contents

Chapter 1

Introduction

Astronomical spectroscopy, as known, is a means of studying various astronomical sources (radiating EM waves) using the techniques of spectroscopy to determine the source's electromagnetic spectrum. A stellar spectrum (spectral energy distribution) is useful in determining various stellar properties such as their effective temperature (T_{eff}), surface gravity ($log(g)$), chemical composition, radius (provided distance estimates to the source is available), motion of the source with respect to observer with Doppler shift measurements, luminosity and many more. Spectroscopy, in general can be used to determine physical and chemical properties of various astronomical sources, not just stellar systems.[58]

Astronomical spectroscopy, as a pipeline, begins with data acquisition and data reduction, followed by inference of properties of the source being observed from the data acquired and finally interpreting the results obtained. Traditionally, the spectroscopy in astronomy was limited to equivalent width measurements and determination of stellar properties from the same. As this method only utilized some portions of the spectral information available, it hints to the possibility to extract much more information regarding the source using the complete spectrum. Hence, the method of synthetic spectrum matching (template matching) to observed spectrum was introduced, where the synthetic spectra for each type of star is built by modelling its stellar atmosphere and generating the model stellar spectrum. This model spectrum so generated is matched with the observed spectrum to infer the physical and chemical properties of the star. By this template matching method, one can use a cost function (parameterizing the errors in the fit)

to be minimized to minimize the errors in the fit. Further, the set of values of each parameter can be varied to obtain a synthetic spectrum that best matches the observed spectrum and infer source properties from the model parameter values. This method helps decide to determine the parameter values from the synthetic spectrum method (by constraining the parameter space being explored) or to determine the same from other methods and plug in the same in the model.[48]

In this report, the results obtained by fitting synthetic spectrum generated with Kurucz models to observed stellar spectrum is presented. The computer program ALTAS9 written by Dr. Robert L. Kurucz calculates model stellar atmospheres in radiative and convective equilibrium for the complete range of stellar temperatures[52]. The computer program SYNTHE is used to compute the synthetic spectrum from the ATLAS9 model atmosphere. A Python library named PySynphot is used to access the model spectra directly and use the same for interpolation and fitting observed spectrum.

1.1 Objective

The main objectives of this internship project are is to determine the efficiency of the Kurucz model spectrum in fitting model flux distribution to observed flux distribution for various types of stars.

Chapter 2

Literature Survey

The literature survey was performed to get an insight into the real life situations where model atmospheres play a crucial role in obtaining the properties of the stellar systems (stars). In general, theoretical models find application in determining properties of various astronomical sources, by template matching method.

The model atmospheres and the flux distribution obtained by analytical and numerical means are useful in classification of astronomical sources. The most successful approaches to classification have used methods from machine learning (Bailer-Jones 2001).In this approach, the spread of spectra (of stars belonging to different spectral types and sub-types) in the set of training samples affects the training of the model/classifier, with in turn affects the performance of the classifier on test set of spectra.

Various theoretical models are used for population synthesis, predicting theoretical evolutionary tracks (in studies related to cluster of stars like globular clusters, star clusters, etc.,), estimating stellar physical properties, like radius (given the distance to the source), effective temperature, color temperature, surface gravity, mass (if surface gravity and radius is known) as well as the chemical properties like metallicity, metal abundance, and many more.

Further, the match between the theoretical model's predictions (like spectrum, physical and chemical properties) and observations over a wide range of observational data samples indicates that the theoretical basis on which the model is built is mostly correct. As in the field of Astronomy, the

scientists can in no way perform controlled experiments on the sources, the only way one can infer about the physics of the same is through theoretical and semi/fully-empirical models.

In the context of stellar atmosphere modelling, various astrophysicists have worked on building their own models. Much work is done in relaxing various approximations (such as plane parallel atmosphere, existence of LTE, and many alike) and building model atmospheres which best represent the true stellar atmospheres to as high degree of accuracy as possible. Some of the commonly used model atmospheres are: Kurucz Models, NextGen, Phoenix, BaSTI models, TLUSTY, MARCS, and many more. Also, each of the models attempts to simulate the atmosphere as on different types of stars - main sequence stars, horizontal branch stars, brown dwarfs, giant stars, etc.,

In the context of synthetic spectrum fitting, much work is done in collecting the line list and creating a database of spectral lines. Some of the commonly used line list database are: Vienna Atomic Line Database (VALD), National Institute of Standards and Technology (NIST) Database and various authors have also published their database of line list, such as Kurucz line list. This along with the model atmospheres can be used to obtain the synthetic spectrum for a source defined by a set of physical parameters (effective temperature: T_{eff}, surface gravity: log(g), metallicity: [Fe/H],microturbulent velocity: ζ, and alike).

2.1 Literature Review

The flux distribution output by ATLAS9 (Kurucz Models) obtained by variation in effective temperature and surface gravity were fit to observed flux distribution of stars of various spectral and luminosity classes and solar metallicity (**Straižys, Lazauskaitė and Valiauga, 1997**). It was found that Kurucz models (1995) predict model flux distribution which matches the mean flux distribution of main sequence, subgiant and supergiant stars (O7 to M0 spectral classes and V to Ia luminosity classes). Only visible and near UV portion of the observed spectra were considered for analysis. Largest differences are found in UV region in early type stars (especially, B-supergiants) and the fit was found to be unacceptable for K7-M type stars

of all luminosity classes[45].

The flux distribution of synthetic spectra from Kurucz model atmospheres were compared with that observed from metal-deficient stars of the blue horizontal-branch (BHB), F–G–K subdwarf (SD) and G–K giant (MDG) types (**Straižys, Lazauskaitė and Valiauga, 2002**). The authors conclude that the Kurucz metal-deficient models with $T_{eff} > 4500K$ fit the observed flux distribution for BHB, extreme SDs and extreme MDGs, when the observational errors are considered. The largest differences are found in the UV wavelength range for SDs and cool MDGs. The influence of errors of surface gravities, effective temperatures and metallicities is estimated[46].

The model atmosphere by Kurucz is widely used by various researchers in modelling the stellar atmosphere and use the same to generate the (synthetic) spectrum of the star for fitting observed spectra of stars and infer its properties.

A library of high resolution Kurucz spectra in the range 3000-10000$\mathring{A}$ was generated by **T. Murphy and A. Meiksin (2004)**[32]. It consists of 6410 synthetic spectra with $\frac{\lambda}{\Delta\lambda} = 250000$ generated using Kurucz 1993 model atmospheres. The library contains spectra for wavelength between 3000$\mathring{A}$ and 10000$\mathring{A}$, with log(g) ranging from 0.0 to 5.0 in steps of 0.5 dex, 54 effective temperatures between 5250K and 50000K along with metallicity ranging from -5.0 to 1.0 in steps of 0.5 dex. The high resolution library of spectra is generated for application in population synthesis studies and physical parameterization of stellar spectra.

Similarly, various collaborators have generated libraries of 711 synthetic spectra with help of Kurucz model atmospheres. **Chavez, Malagnini and Morossi (1997)**[12] generated a library of synthetic spectra in wavelength range 4850-5400$\mathring{A}$ for log(g) ranging from 1.0 to 5.0 in steps of 0.5 dex, 11 effective temperatures between 4000K and 8000K and 7 metallicity values between -1.0 and 0.5 dex. The library is dedicated for application in analysis of composite stellar populations on basis of spectral features in observed composite light of clusters and galaxies.

Castelli and Munari (2000)[9] generated a library of 698 synthetic spectra with a resolution of 20000 in the wavelength range 7650-8750$\mathring{A}$ for use

with GAIA spectra. The metallicity range explored is -2.5$\leq [Z/Z_{\odot}] \leq$ +0.5, that of surface gravity between 2.0 and 4.5 and effective temperature between 7750K and 50000K.

The above list of researches and analysis is non-exhaustive. Various authors have analysed different stellar atmosphere models on different datasets, which have not been included here.

Chapter 3

Theory

3.1 Kurucz Models

Any model calculations begins with certain assumptions. The following are the set of assumptions and approximations made in Kurucz models to simplify the problem physically and computationally[52].

1. Steady state approximation of atmosphere
2. There is no source or sink in the atmosphere or star, hence, the net flux throughout the atmosphere is constant.
3. The atmosphere is homogeneous except in radial direction (from center of star).
4. The effects due to magnetic fields, stellar spots, granules, etc are ignored.
5. Plane parallel atmosphere approximation, i.e., the height of atmosphere is much less than the radius of the star
6. Hydrostatic equilibrium with no relative motion between the layers of the atmosphere
7. Abundance of atoms is constant throughout the atmosphere.
8. The stellar atmosphere is in thermodynamic equilibrium (which includes, mechanical, chemical and thermal equilibrium)

9. There is on influx of radiation from the top of the atmosphere (i.e., no source in the vicinity of the stellar system)

The model atmosphere is found by iterative procedure. The temperature is guessed at a set of depth points in the stellar atmosphere and the physical properties of the stellar atmosphere - pressure, opacity, and number density values are calculated at same set of points. From the same, the radiation field and convective flux is determined at each depth point. In general, a mismatch is found between the total flux and prescribed constant flux, hence with help of a temperature correction scheme, the temperature at each depth point is varied to reduce the flux mis-match. The above described procedure is iterated until convergence (total flux equals prescribed flux within tolerance limit). Often, since number density and pressure are weakly dependent on radiation field, only the temperature is carried over successive iterations.

Kurucz models define the depth points (of plane parallel layers) in terms of the Rosseland optical depth. A good way to get an initial guess of model temperature at each depth points is to scale the pre-existing values by the ratio of effective temperatures ($\frac{T_{eff}^{new}}{T_{eff}^{old}}$). The Rosseland optical depth is well suited for the above mentioned type of scaling (where, for $\kappa \propto \nu^{-n}$ implies, $\kappa \propto T^{-n}$). The Rosseland mean opacity is defined as weighted average of opacity with temperature derivative of the Planck distribution as the weighting function.

$$\frac{1}{\kappa} = \frac{\int_0^\infty \kappa_\nu^{-1} u(\nu, T) d\nu}{\int_0^\infty u(\nu, T) d\nu}$$

The solar abundance values for each element are borrowed from Grevesse & Sauval (1998 Space. Sci. Rev.,85,161; GS98). The TiO lines used are those from Schwenke (1998, Faraday Discuss., 109,321). H_2O lines [34] and of the HI-HI and HI-H+ quasi-molecular absorptions near 1600 Å and 1400 Å [1] are also included in the model atmosphere computation.

The solar scaled abundances values are used in the model, with no enhancement factor. Under the assumption that the abundance of Hydrogen of star (under consideration) is equal to that of solar value, we get that $[Fe/H] = [M/H] = log(Z/Z_\odot)$ (using $[Fe/H] = log(Z/Z_\odot) - log(X/X_\odot) -$

Γ[43]).

```
TEFF   5777.  GRAVITY 4.43770 LTE
TITLE  [0.0] VTURB=1.0 KM/SEC  L/H=1.25 NOVER NEW ODF
 OPACITY IFOP 1 1 1 1 1 1 1 1 1 1 1 1 1 0 1 0 0 0 0 0
 CONVECTION ON   1.25 TURBULENCE OFF  0.00  0.00  0.00  0.00
ABUNDANCE SCALE   1.00000 ABUNDANCE CHANGE 1 0.92040 2 0.07834
 ABUNDANCE CHANGE  3 -10.94  4 -10.64  5  -9.49  6  -3.52  7  -4.12  8  -3.21
 ABUNDANCE CHANGE  9  -7.48 10  -3.96 11  -5.71 12  -4.46 13  -5.57 14  -4.49
 ABUNDANCE CHANGE 15  -6.59 16  -4.71 17  -6.54 18  -5.64 19  -6.92 20  -5.68
 ABUNDANCE CHANGE 21  -8.87 22  -7.02 23  -8.04 24  -6.37 25  -6.65 26  -4.54
 ABUNDANCE CHANGE 27  -7.12 28  -5.79 29  -7.83 30  -7.44 31  -9.16 32  -8.63
 ABUNDANCE CHANGE 33  -9.67 34  -8.63 35  -9.41 36  -8.73 37  -9.44 38  -9.07
 ABUNDANCE CHANGE 39  -9.80 40  -9.44 41 -10.62 42 -10.12 43 -20.00 44 -10.20
 ABUNDANCE CHANGE 45 -10.92 46 -10.35 47 -11.10 48 -10.27 49 -10.38 50 -10.04
 ABUNDANCE CHANGE 51 -11.04 52  -9.80 53 -10.53 54  -9.87 55 -10.91 56  -9.91
 ABUNDANCE CHANGE 57 -10.87 58 -10.46 59 -11.33 60 -10.54 61 -20.00 62 -11.03
 ABUNDANCE CHANGE 63 -11.53 64 -10.92 65 -11.69 66 -10.90 67 -11.78 68 -11.11
 ABUNDANCE CHANGE 69 -12.04 70 -10.96 71 -11.98 72 -11.16 73 -12.17 74 -10.93
 ABUNDANCE CHANGE 75 -11.76 76 -10.59 77 -10.69 78 -10.24 79 -11.03 80 -10.91
 ABUNDANCE CHANGE 81 -11.14 82 -10.09 83 -11.33 84 -20.00 85 -20.00 86 -20.00
 ABUNDANCE CHANGE 87 -20.00 88 -20.00 89 -20.00 90 -11.95 91 -20.00 92 -12.54
 ABUNDANCE CHANGE 93 -20.00 94 -20.00 95 -20.00 96 -20.00 97 -20.00 98 -20.00
 ABUNDANCE CHANGE 99 -20.00
READ DECK6 72 RHOX,T,P,XNE,ABROSS,ACCRAD,VTURB, FLXCNV,VCONV,VELSND
 5.85641157E-04   3650.6 1.604E+01 2.691E+09 2.277E-04 4.614E-02 1.000E+05 0.000E+00 0.000E+00 6.696E+05
 7.64075733E-04   3679.3 2.093E+01 3.460E+09 2.708E-04 5.246E-02 1.000E+05 0.000E+00 0.000E+00 6.624E+05
 9.64357866E-04   3708.1 2.642E+01 4.323E+09 3.215E-04 5.875E-02 1.000E+05 0.000E+00 0.000E+00 6.581E+05
```

Figure 3.1: Example of Kurucz Model Atmosphere file

As can be seen in the Figure 3.1, the details of the model are printed in the headers along with other details required for computation of model atmosphere. Any given model atmosphere file can be used (as an initial guess of atmospheric properties) to compute another model atmosphere corresponding to different set of parameters.

The first line displays the effective temperature and surface gravity (log(g), where g is in cgs units). "LTE" at the end of first line specifies that the model atmosphere is in local thermodynamic equilibrium. The second line displays the metal abundance in square brackets followed by the microturbulent velocity (in km/s). It displays the mixing-length to the pressure scale height ratio (l/H_p) value, which, if non-zero, indicates that the convection option is on. The word "NOVER" specifies that the overshooting option is switched off (NOVER = No Overshoot) and at last is the work "NEWODF" to indicate that updated version of opacity distribution function is used in generating the model atmosphere.

The next few lines specify the element number followed by the abundance ($log_{10}(\frac{N_{el}}{N_H}) = A - 12$). Next set of lines corresponds to the plane parallal

atmosphere layers's physical properties. The columns are, in the order,

1. (72) number of layers in the model stellar atmosphere
2. (RHOX) mass depth
3. (T) temperature (at each depth)
4. (P) gas pressure
5. (XNE) electron density
6. (ABROSS) Rosseland mean absorption coefficient
7. (ACCRAD) radiated pressure
8. (VTURB) micro-turbulent velocity (in m/s)
9. (FLXCNV) amount of flux transported by convection
10. (VCONV) convective velocity
11. (VELSND) sound velocity

One of the challenges in model atmosphere calculations is the treatment of a large number of atomic and molecular lines typically found in a stellar spectrum. In applications requiring only the flux information in broad wavelength intervals, the same can be obtained from opacity distribution functions (ODFs). ODF is obtained by splitting the entire wavelength range into bins. The total opacity in each bin is the sum of the line and continuum opacity. Under LTE assumption, the opacity mainly depends on the wavelength, pressure, temperature and the velocity distribution in the atmosphere (to some extent). In 1D models, the velocity distribution is quantified by the microturbulent velocity, which allows the ODF to be pre-tabulated on a grid of pressures and temperatures, with intermediate values obtained by interpolation. Castelli & Kurucz (2004) employed 12 values for approximating opacity within the bin to synthesize spectra over a broad range of stellar parameters.

The model atmospheres in Kurucz grid of models use Rosseland opacity. Rosseland opacity is defined with temperature derivative of Planck distribution function as the weight function. It is derived in diffusion approximation

to radiative transport equation [16] which is valid under local thermodynamic equilibrium conditions.

3.1.1 Comparison between Castelli and Kurucz (2004) and Kurucz (1993) models

The major improvements from previous opacity distribution functions listed in Castelli & Kurucz 2003[11] are [53] :

1. The replacement of the solar abundances from Andres & Grevesse (1989, GCA,53,197; AG89) with those from Grevesse & Sauval (1998 Space. Sci. Rev.,85,161; GS98).

2. The replacement of the TiO lines provided by Kurucz (1993) with the TiO lines from Schwenke (1998, Faraday Discuss., 109,321). Addition of the H_2O lines (Partridge & Schwenke 1997, J. Chem. Phys., 106, 4618) and of the HI-HI and HI-H+ quasi-molecular absorptions near 1600 Å and 1400 Å (Allard et al. 1998, A&A, 335,1124), as distributed by Kurucz 1999a, 1999b. Extended molecular list and corrected previous bugs in Kurucz line lists.

Preliminary comparisons of flux densities have shown that the differences in solar abundances used, have no significant effect except when additional absorptions introduced in the new-ODFs play an important role. Exceptional differences which increase with decreasing gravity and/or metallicity can be observed in the 1250-2000 $\mathring{A}$ region for $T_{eff} \in$ (7000, 9000) K, which have roots in $HI - H^+$ and $HI - HI$ quasi-molecular absorptions.

The new TiO line list, the addition of H_2O lines and some improvements in the molecular data have greatly modified the flux density of models cooler than 4500 K. The new TiO line list, the addition of H_2O lines and some improvements in the molecular data have greatly modified the energy distributions of models cooler than 4500 K.

Color indices U-B from new-ODF models are redder than the indices from the old-ODF models for $T_{eff} < 6500K$. The difference increases with decreasing T_{eff} . For instance, the difference for U-B amounts to 75 K when the model T_{eff} =5750 K, logg=4.5, [M/H]=0.0, ξ=2 km/s is considered.

Both (B-V) from new-ODFs are redder than those from old-ODFs for $T_{eff} <$ 4500K.[11]

3.2 PySynphot

Astrolib PySynphot[54] is an object-oriented replacement for STSDAS SYNPHOT synthetic photometry package in IRAF. It is used to simulate photometric data and spectra as observed with the Hubble Space Telescope (HST). Data files needed for calculations involving synthetic spectra are provided, of which Castelli & Kurucz (2004) stellar atlas is used in this project. The synthetic spectra is stored in "FITS" files. The models with same abundance (or metallicity, which ranges from -2.5 to 0.5 dex, in steps of 0.5 dex and one at 0.2 dex) are stored in the same directory. The individual FITS file is designated by the model effective temperature it represents and contains 12 columns, first column being wavelength in $\mathring{A}$ and the remaining 11 columns contain the flux values for 11 different values of $log(g)$ starting from 0.0 to 5.0 in steps of 0.5. The surface flux values returned are in FLAM units ($erg/s/cm^2/\mathring{A}$). The "cat" function can be used to get the model nearest to the set of values of input parameters specified (as arguments to it) whereas, the "icat" function can be used to get the interpolated model. Models with a micro-turbulent velocity of 2km/s are used in this project.

3.3 Spectres

In case of fitting model spectrum to that observed, one can encounter a situation where the observed spectrum (with uncertainty values) has lower number of samples points in a given wavelength range than that of model, in which case a simple interpolation (as in the opposite case, with model spectrum) cannot be sufficient. In such cases, it is necessary to accurately re-sample the flux data along with the associated uncertainty values. In such cases, the SpectRes Python function is helpful in efficiently re-sampling spectra and their associated uncertainties onto an arbitrary wavelength grid. The function works with any grid of wavelength values, including non-uniform sampling, and preserves the integrated flux. This may be of use for binning data to increase the signal to noise ratio, obtaining synthetic photometry,

or, as mentioned above, re-sampling model spectra to match the sampling of observational data.[8]

Chapter 4

Methodology

The present chapter is dedicated to explain the conceptual overview of the synthetic spectrum fitting. The theory and algorithms are described with aid of diagrams and flow charts.

4.1 Data

In this project, 2 different datasets were used, as briefed below:

1. **STELIB Stellar Spectral Library**[21]: The spectra in this dataset was assembled from the observational data from two telescopes -

   (a) 1m Jacobus Kaptein Telescope (JKT), Roque de los Muchachos Observatory, La Palma, Canary Islands, Spain, between 1994 March 28 and April 4 with Richardson-Brealey Spectrograph (600 lines/mm grating) and EEV7 1242X1152 CCD with a 22.5 µm pixel and a slit width of 1.5".
   This resulted in a dispersion of 1.7Å/pixel and a resolution of about 3Å FWHM. During this run 1000 spectra were obtained on about 200 stars.

   (b) 2.3m of the Australian National University at Siding Spring (SSO), Australia, between 1994 December 25 and 31 with Double Beam Spectrograph (600 lines/mm grating) and 2 1024×1024 CCD's with a dispersion of 1.1Å/pixel (15 µm pixels) and slit width of 2". The spectral resolution is about 3Å FWHM.

Most stars were originally selected from the catalogue of Cayrel de Strobel et al.(1992) according to the value of [Fe/H]. Additional samples of 62 and 45 stars were selected to include targets with either near-IR spectra (from Lançon & Rocca-Volmerange 1992) and/or UV data (from IUE) respectively.

Data Reduction: The basic data reduction was performed with IRAF software. The wavelength calibration was done using arc spectra from a Cu-Ne lamp for the JKT data and from He-Ar, Ar-Ne and Cu-Ar lamps for the SSO data. The typical number of lines used was 30 to 50. The rms of the residuals was found to be $\sim 0.1\mathring{A}$.

For applying extinction correction, a set of standard stars' spectra were used. The examination of these spectra observed from JKT revealed strongly varying atmospheric extinction during the observations. The normal atmospheric extinction is modeled by the mean atmospheric extinction versus wavelength curve and the airmass during observation. The "abnormal" extinction, possibly due to dust, is likely to change rapidly during one night. This effect was accounted (calibrated) for by using any observed star as a photometric standard star.

The SSO Spectra were reduced using standard procedures for flux calibration. The efficiency of calibration was found from the goodness of fit with the standard stars' published SEDs.

This resulted in 257 stellar spectra in FITS format re-sampled with a step of 1Å per pixel. The library is available in two different forms:

(a) the "raw" data, including the combined spectra as coming out of the calibration process

(b) the data corrected for interstellar reddening using the empirical extinction function of Cardelli et al. (1989).

The observational flux distribution data has wavelength in units of $\mathring{A}$ and flux density in units of $erg/s/cm^2/\mathring{A}$. The observational data from STELIB spectral library, suffers a significant drop in flux in the

wavelength range 7500$\mathring{A}$ to 7750$\mathring{A}$ (close to 7600$\mathring{A}$) which can be identified as the telluric lines in the A band, mainly due to absorption by O_2.

2. **IRTF Spectral Library[55]**: The NASA InfraRed Telescope Facility(IRTF) Spectral Library is a collection of 0.8-5.0 µm mostly stellar spectra observed at a resolving power $\sim$ 2000 with the medium-resolution spectrograph, SpeX, at the NASA IRTF on Mauna Kea. The dataset covers mainly solar-metallicity late-type stars with spectral types between F and M and luminosity classes between I and V, but also includes AGB stars, carbon and S stars, and L and T dwarfs. It also include spectra of the giant planets, Jupiter, Saturn, Uranus, and Neptune. Later updates will add Wolf-Rayet, O, B, and A stars.

   The resolving power, R $\sim$ 2000 from 0.8-2.5 µm and R $\sim$ 2500 from 2.5-5.2 µm with a S/N ratio $\sim$ 100 for λ <4 µm.The flux calibration is achieved using Two Micron All Sky Survey (2MASS) photometry.

   The spectrograph employs an Aladdin 3 1024 X 1024 InSb array and uses narrow slits and a spatial scale of 0".15/pixel for optimum sensitivity on point sources[42].

   The observational spectrum data has wavelength in units of μm and flux in units of $W/m^2/\mu m$.

As the motive of this internship project is to analyse the Kurucz models and determine its performance in fitting synthetic spectrum to observed spectrum, only those sources in the dataset were considered, for which the values of the parameters being estimated (T_{eff}, log(g), and metal abundance) were available from publication by various authors.

4.2 Kurucz Model Flux Distribution Fitting Pipeline

This section describes the method by which the synthetic spectrum was fit to the observed spectrum.

The distance estimate to the source, whose spectrum is being fit with model spectrum was determined (along with uncertainty values) using the parallax values obtained from SIMBAD database. This was used in the estimation of the radius of the star, though the dilution factor, $M_d = (\frac{R}{D})^2$, which is multiplied with the model surface flux values to obtain an amplitude (approximately) matching with observed spectrum.

For estimating effective temperature, the values published by various authors was used. The precision of grid search was limited to 100K. The values around that published (in research papers) were searched with above mentioned precision. In case of the temperature uncertainty values being available and more than 100K, the range of temperature explored is increased, with minimum and maximum being the minimum and maximum temperature, considering the uncertainty values. (essentially, floor of minimum temperature and ceil of maximum temperature)

For estimating surface gravity, the values around that quoted by the authors ($\pm$0.1 dex) were explored and half the grid step size is reported as the uncertainty value. The metallicity (metal abundance) was also estimated similarly. In case of uncertainty values being mentioned, the values between the floor of minimum metallicity and ceil of maximum temperature, considering the uncertainty values, are explored in step size of 0.1 dex. Finally, similar to surface gravity, half the grid step size is reported as uncertainty value.

4.3 Evaluation Metrices

To measure the goodness of fit the following cost functions were considered.

1. **Chi-Squared Value** was used in cases where the observational flux uncertainty (or error) values were not available. $\chi^2 = \sum_i \frac{(O_i - C_i)^2}{C_i}$ where, O_i are the observational flux values, C_i are the expected flux values (i.e., flux value predicted from Kurucz models).

2. **Reduced Chi-Squared Value** was used in cases where the data included the observational flux uncertainty values, with number of de-

grees of $\nu = n - m$, where, m is the number of parameters being estimated, which here is 4.
$\chi^2_\nu = \frac{\chi^2}{\nu}$
$\chi^2 = \sum_i \frac{(O_i - C_i)^2}{\sigma_i^2}$
where, O_i, C_i are same as mentioned above and σ_i is the observational flux uncertainty value.

3. **Total Percentage residual** value was used in the cost function with a free weight parameter (λ). $\%TotalResidual = \sum_i \frac{|O_i - C_i|}{|O_i|} \times 100\%$

The final cost function, (reduced) Chi-Square value along with the weighted total percentage residual, was used to minimization during the search.

Chapter 5

Implementation

The analysis was performed using Python (3.6) programming language. The main Python libraries used in this internship project are:

1. PySynphot
2. PyAstronomy
3. scipy
4. astropy
5. matplotlib
6. numpy
7. csv

Scipy's "*chi_square*" function was used to get chi-squared values of fit. In cases where observational uncertainty values were available, reduced chi-square value was computed by hand-coding the formula into a (user defined) function, which also returns the corresponding P value by computing it using scipy.stats.chi2.cdf(x,v) function, where x is the reduced chi-square value and v is the number of degrees of freedom, which is the number of data points less the number of parameters being fit (here, 4).

In cases where the observational data was available in FITS file, PyAstronomy's read1dFitsSpec function was used and in cases where the same was available in ascii file, simple file handling facility of Python was used. The

distance to the sources were computed using the parallax values (saved in an ascii file) along with the uncertainty values which was used to determine the radius of the sources.

In order to minimize both percentage residual and the chi-square values, without affecting the P value, the cost function was defined to be weighted sum of the two values, were the weight parameter (which is multiplied to the percentage mean residual value), λ was set to 10^{-10} in case of fitting Kurucz models to STELIB observational flux distribution(s) and the same was set to 1000 in case of fitting model flux distribution to IRTF data. The value of the (relative) weight parameter was set so as to make the order of magnitude of both the percentage residual and chi-square values same.

The model flux distributions were obtained using PySynphot's Icat function, by passing the name of the model (here, "ck04models"), values of effective temperature, metallicity and surface gravity as function input arguments, in the order. The Icat function returns the interpolated flux distribution for the given set of model parameters from pre-exiting flux distributions for a grid of parameters (details mentioned in the section "PySynphot" in the chapter "Theory").

The number of data points in the observational data and model data are compared. In case the former being greater than latter, simple interpolation (using numpy's "interp" function) is performed on the model flux distribution over the wavelengths in observational data. Whereas in case of the situation being reverse, the next step depends on the type of data, as described below:

1. Observational flux uncertainty values available: In that case, it is necessary to interpolate the uncertainty values along with the flux values, for which, "spectres" library's spectres function is used

2. Observational flux uncertainty values un-available: In that case, simple interpolation (similar to that performed on model data) over the model data wavelength values suffices.

Thus, using the above mentioned procedure, the grid search is performed over the range of parameters being estimated.

Next, the photometric flux and magnitude values are determined using the transmission curves and their values at effective wavelength.

For analysis on STELIB dataset, due to unavailability of the Johnson UBVRI filter curves used in the Lausanne database (from which, the photoelectric photometric values are taken in J.-F. Le Borgne et al. (2003)), the ones closest to those were used, which here is Johnson-Cousins UBVRI filter curves[56]. The photometric flux when observed through each filter is computed by convolving and integrating the model flux distribution with filter transmission curves. Then, the zero-magnitude flux in each band[20] is used to calculate the apparent magnitude of the source in each wavebands. The effective wavelength and zero-magnitude flux values used in the analysis are given in the Table 5.2

Band	λ_{eff} (μm)	Flux at m=0 ($10^{-13}\frac{W}{cm^2.\mu m}$)
J	1.25	3.06
H	1.65	1.13
Ks	2.16	4.27

Table 5.1: J, H and Ks Band Filter Characteristics Used[20][57][51]

Band	λ_{eff} ($\mathring{A}$)	FWHM ($\mathring{A}$)	Flux at m=0 ($10^{-9}\frac{erg}{s.cm^2.\mathring{A}}$)
U	3656	340	4.19
B	4353	781	6.60
V	5477	991	3.61
R	6349	1065.6	2.25
I	8797	2892	1.22

Table 5.2: U, B, V, R and I Band Filter Characteristics Used[20][56]

With the V Band (synthetic) apparent magnitude and the distance estimate to the star being available the absolute magnitude is estimated using distance modulus formula (m-M = -5 + 5log(d(in pc))). Finally, the model and observed flux distributions in different wavebands are plotted in same plot(s) to ease visual comparison. The apparent magnitude and photometric flux values in each waveband are stored in separate csv files.

For analysis on NASA IRTF dataset, the 2MASS J, H and Ks filter curves[57] were used to find J, H and Ks band magnitudes. The effective wavelength and zero-magnitude flux values used in the analysis are given in the Table 5.1

Chapter 6

Results and Analysis

6.1 STELIB Data Analysis

The dataset that has been taken for the analysis is retrieved from STELIB: A Spectral Library for stellar spectra[21]. Minimum of 5 sources belonging to each of the five spectral classes (B, A, F, G, and K) in the dataset, for which all the fit parameters values were available in the paper "STELIB: a library of stellar spectra at R$\sim$2000" by J.-F. Le Borgne et al. (2003). Sources which are isolated stars are considered excluding the binary stars or double stars. The results of the analysis performed on the performance of the Kurucz models in fitting model flux distribution to the observed flux distribution is presented in this section. Pictorial representation of various results obtained is presented for enhanced clarity.

Table 6.1 contains the information regarding the values of the fit parameters obtained by fitting Kurucz model spectral energy density with observed flux data and the same as obtained from research papers. The name of the source (as in Henry Draper Catalogue) and their spectral type (as given in J.-F. Le Borgne et al. (2003)[21] and SIMBAD database[30]) is also mentioned. Also, in the flux distribution available, the U band is not completely covered as the data includes the flux density values only above 3500, hence, the contribution to the photometric flux in U band is less than the observed values (thus, apparent magnitude is higher than the observed values).

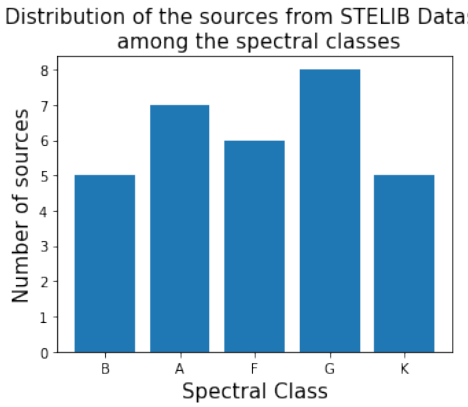

Figure 6.1: Number of sources in considered data subset per spectral class

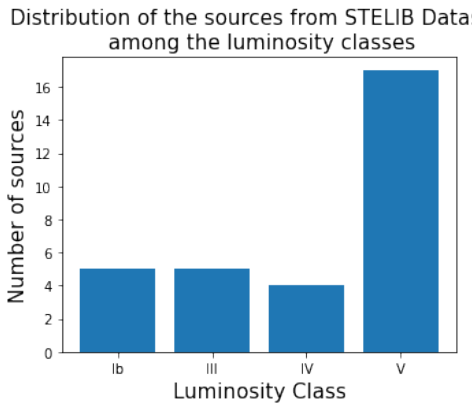

Figure 6.2: Number of sources in considered data subset per luminosity class

Throughout the analysis, the effective temperature of the fit was limited to 100K, surface gravity and metallicity to 0.1 dex and radius (expressed in terms of faction of radius of sun) to first decimal place.

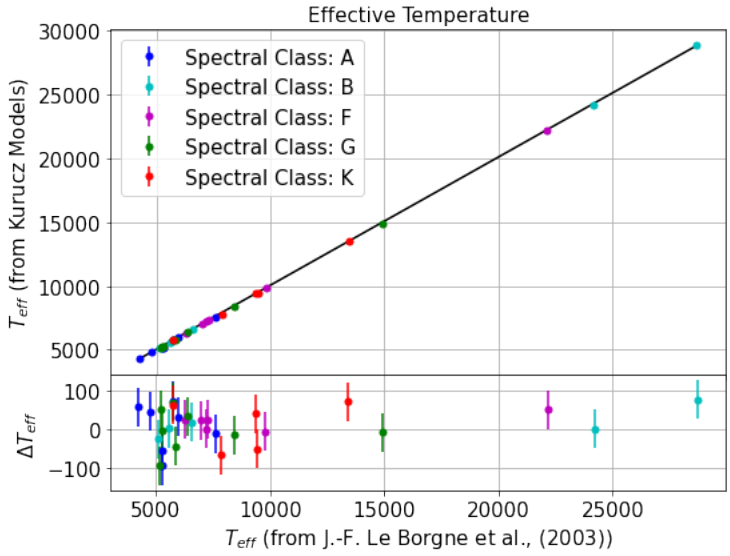

Figure 6.3: Comparison between fit and published values of T_{eff}

We observe from the comparison plot of T_{eff} (Figure 6.3) that when fit

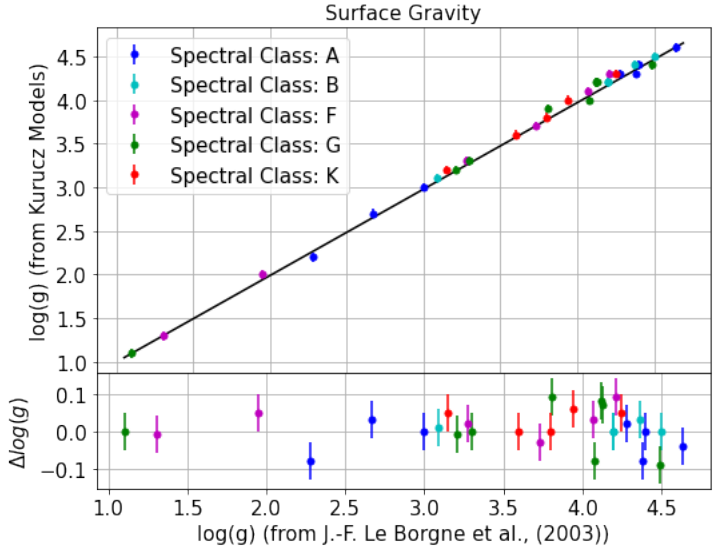

Figure 6.4: Comparison between fit and published values of $log(g)$

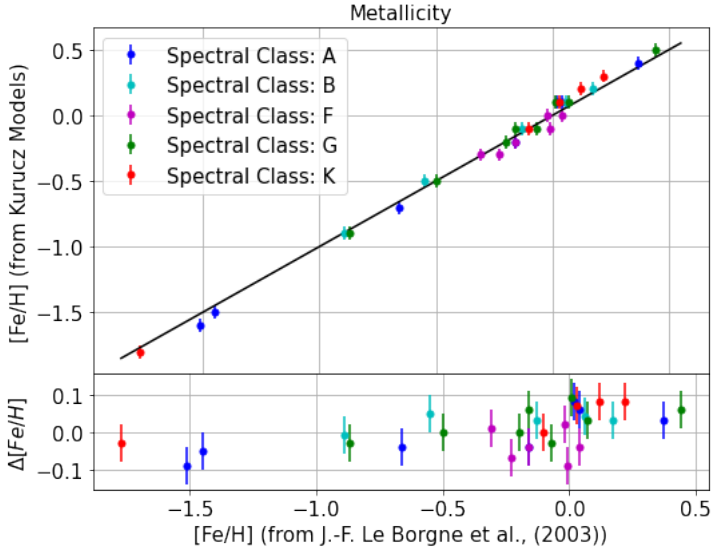

Figure 6.5: Comparison between fit and published values of $[Fe/H]$

Kurucz model flux distribution with that observed (of main sequence, giants and sub giants) the effective temperature predicted by Kurucz models matches well with that published by J.-F. Le Borgne et al. (2003).

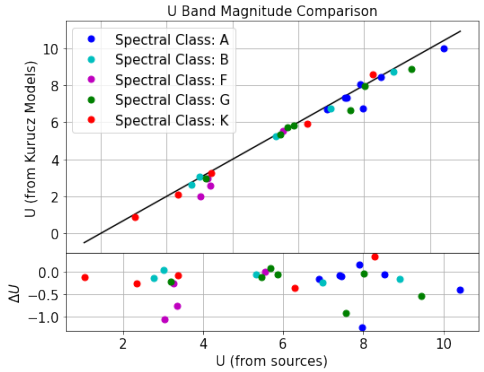

(a) U Band Magnitude Comparison

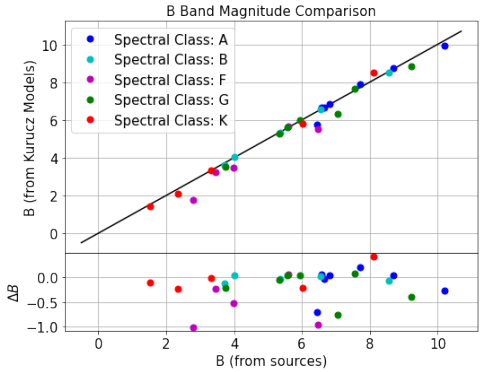

(b) B Band Magnitude Comparison

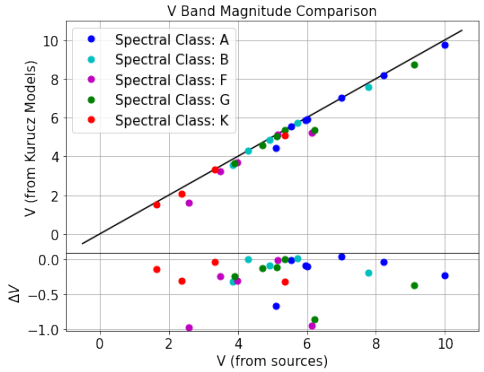

(c) V Band Magnitude Comparison

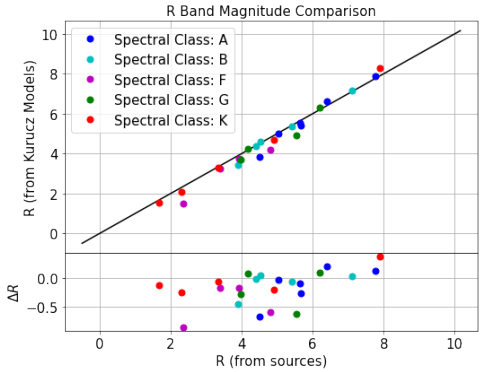

(d) R Band Magnitude Comparison

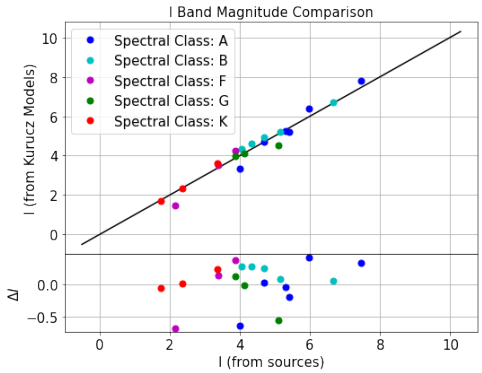

(e) I Band Magnitude Comparison

Figure 6.6: Comparison between synthetic photometric values and observational values (from J.-F. Le Borgne et al. (2003) and SIMBAD database)

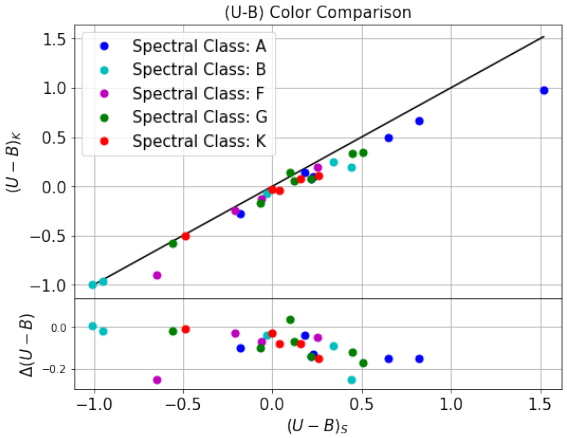

(a) (U-B) color comparison plot

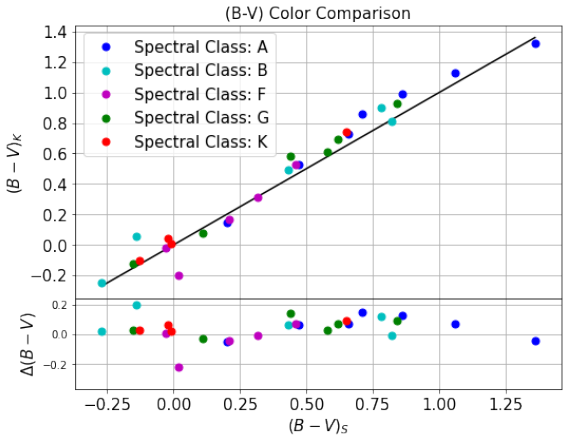

(b) (B-V) color comparison plot

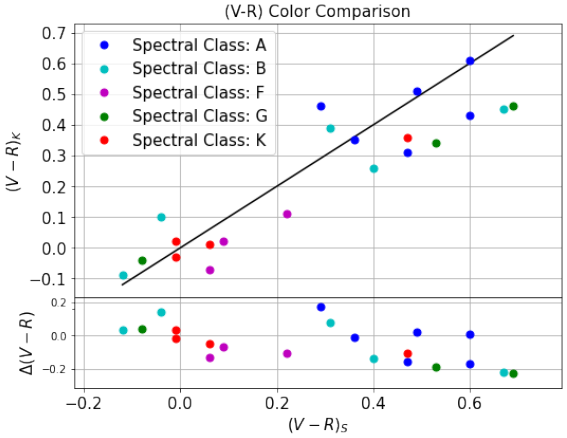

(c) (V-R) color comparison plot

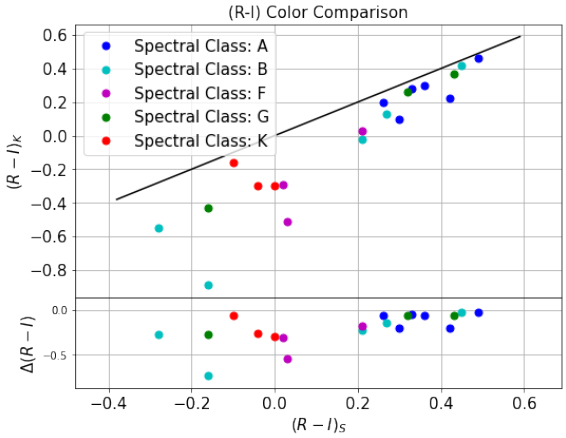

(d) (R-I) color comparison plot

Figure 6.7: Color comparison plot with colors of STELIB spectra on x-axis and corresponding Kurucz synthetic color on y-axis. The solid line (y=x) is included for easing visual comparison.

In general, it was observed that treating the effective temperature as free parameter, though produces physically acceptable values in most cases, there are cases where we can get unacceptable values. Hence, when the effective temperature estimate is not available from photometric (color temperature, two-color method, etc.,) or other methods, with the knowledge of the type of source under consideration, one can use the temperature range given in the literature (with some extension in the range by say, 500K).

In the comparison plot of surface gravity (Figure 6.4), we observe that the value predicted by Kurucz models deviates from that of published value for stars with high surface gravity (dwarf stars, with sub-solar radius and main sequence stars with high surface gravity) and matches well in case of stars with low surface gravity (like giant or supergiant stars) for most of the stars in the dataset considered.

In the comparison plot of metallicity (Figure 6.5), we observe that the spread is small for metallicities away from solar values (by 0.5 dex), whereas high deviation of the model predicted metallicity from that determined independently from other methods is observed close to solar metallicity values (i.e., between -0.5 and +0.5 dex).

Also, we observe a high spread in the values of surface gravity and metallicity (from publications) of the stars included in the data set for analysis. Thus, it would be justified to say that the selection effects in the inclusion of sources belonging to various spectral classes in the dataset is low.

Good match between observed and synthetic photometry is observed in main sequence stars. The percentage mean residual value for these stars (in the dataset) ranges from 5.7% to 15.73%. Main sequence stars belonging to G and F spectral classes are found to have fits with low residual value, whereas high values are found in K types stars. Interestingly, though the goodness of fit is poorer for the main sequence star HD 132142 (K1V star), the match between synthetic and observed photometric magnitudes is still observed to be good (as shown in Figure 6.8 and 6.9).

This is an exception, as it is found that significant deviation is observed in most cases. The I band magnitude is found to be highly mismatched in all the G and F type stars, though, the deviation from observed values of U, B, V and R magnitudes in main sequence star's synthetic photometric magnitudes

```
Best fit model parameters:
Log(g) = 4.5 [0.05]
Teff = 5100 [50]
[Fe/H] = log_10((Fe/H)star/(Fe/H)sun) = -0.5 [0.05]
R = 0.9 [0.05] R_sun
Md = 7.423004641681861e-19
Chi-square value = 2.540465098290934e-10
p value = 1.0
Percentage Mean Residual Value = 15.72693315249696 %

<matplotlib.legend.Legend at 0x7fc40e6810b8>
```

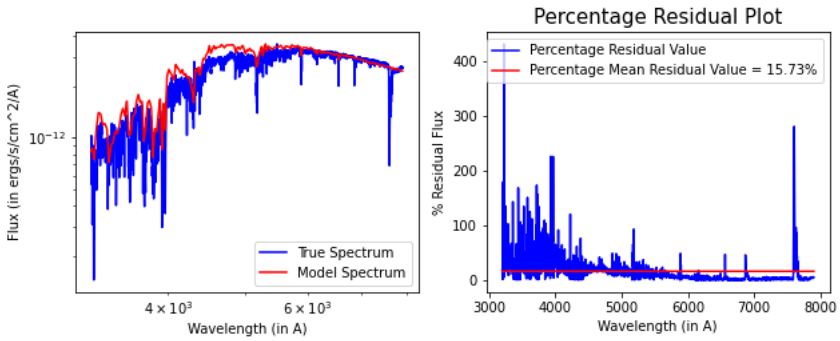

Figure 6.8: Overall fit to HD 132142 (K1V star) - high percentage mean residual value

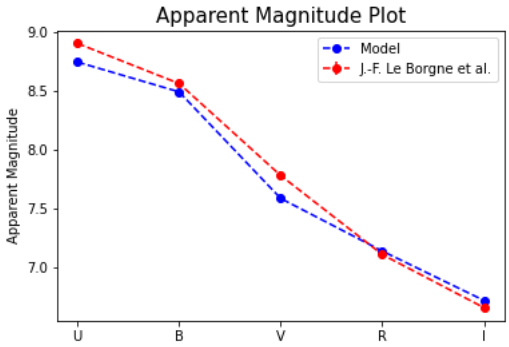

Figure 6.9: Synthetic and observed photometry comparison of HD 132142 (K1V star) - good match inspite of high residual values

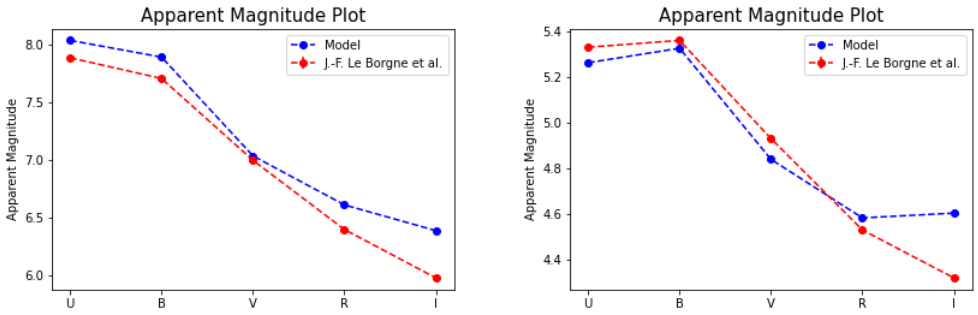

(a) HD 65583 (G8V star) (b) HD 134083 (F5V star)

Figure 6.10: Poor match in I Band Magnitude in main sequence stars

is observed to be relatively (relative to I band magnitude difference) low (as shown in Figure 6.10).

The horizontal branch stars flux distribution are well fit by Kurucz model flux distribution. The form of the flux distribution obtained from the model matches well with the observed flux distribution. Yet, significant mismatch in photometric magnitude is observed in most horizontal branch stars considered. It is observed that the plausible cause for the mismatch is difference in filter transmission curves used, since the magnitudes determined using observational data displays lesser deviation from synthetic photometric magnitudes (see Figure 6.11). Also, the percentage mean residual values are $\sim 6 - 18\%$ (only few outliers with mean residual values $\sim 15 - 18\%$). Also, not all the lines in the Balmer series are well fit by the model SED. This can be traced back to the way in which the opacity is determined in the model (by opacity distribution functions), wherein close by lines are not well models. The software SYNTHE can be used to obtain high resolution spectra of the stars, which is able to fit the lines in Balmer series.

Also, we observe that due to the synthetic spectra having a resolution lower than the observed spectra, not all lines of Balmer series are fit by the model flux distribution. On contrary, we observe that most of the lines in the Paschen series are well fit by the model SED as can be observed from the I band fit of B-A type stars, in which the lines are clearly visible (as can be seen from figure 6.12). In the dataset used, the observed SED of Main Sequence stars doesn't include the data in wavelength range pertaining

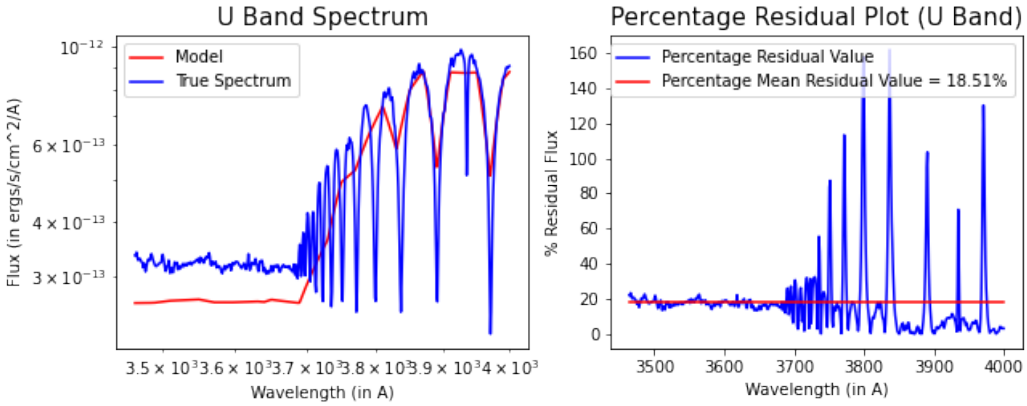

(a) HD 2857 (A2IV star): U Band model flux lesser than observed flux

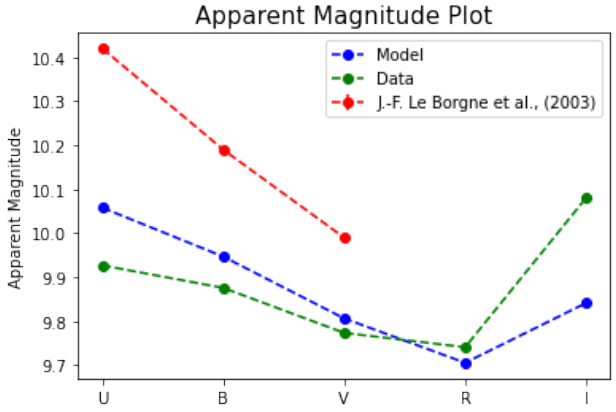

(b) HD 2857 (A2IV star): Synthetic and observed apparent magnitude comparison

Figure 6.11: Horizontal Branch stars - relatively poor fit in U band along with high deviation of synthetic apparent magnitude values from observed values

Paschen lines. We observe telluric absorption by oxygen molecules in Earth's atmosphere in I band - named A band (7600 -7630 A) and R band - named B band (6860 -6890 A).

Hypergiant stars are not fit by Kurucz model, as giving the parameters values of a hypergiant star (for example, HD 26630 - A3Ia star, HD 197345 - A2Ia star) to the "Icat" function does not return any model.

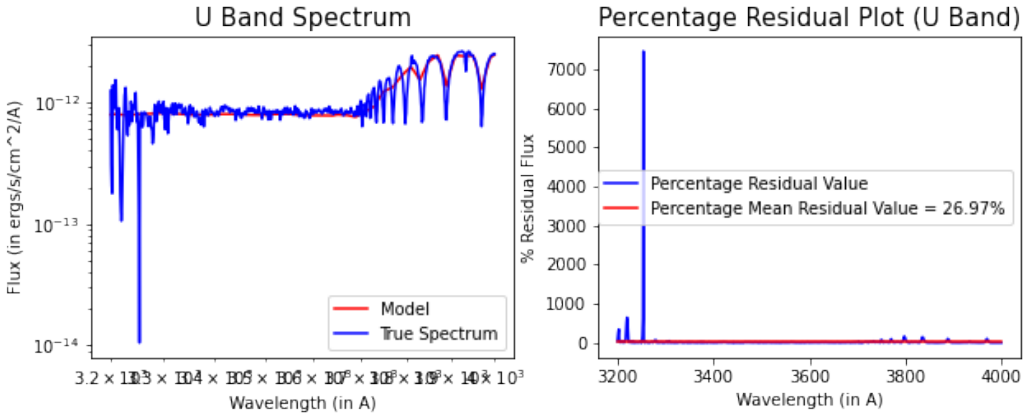

(c) HD 60778 (A1V star): U Band model flux lesser than observed flux

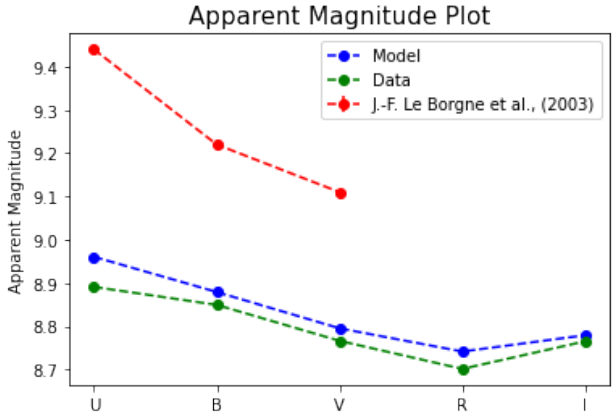

(d) HD 60778 (A1V star): Synthetic and observed apparent magnitude comparison

Figure 6.11: Horizontal Branch stars - relatively poor fit in U band along with high deviation of synthetic apparent magnitude values from observed values

K-type stars flux distritbution are found to be not well fit by Kurucz synthetic spectra (% mean residual values $\sim 10 - 15\%$). Yet, good match is observed between the photometric magnitude values in most of the K-type stars considered (with some outliers).

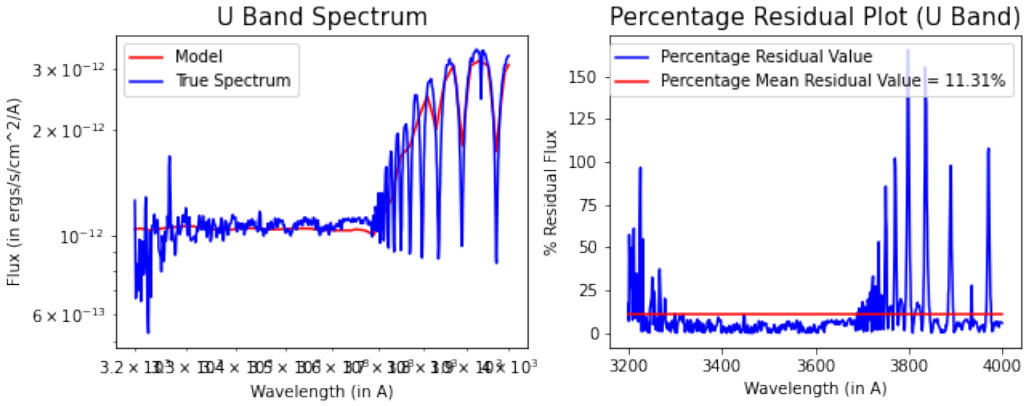

(e) HD 86986 (A1V star): U Band model flux lesser than observed flux

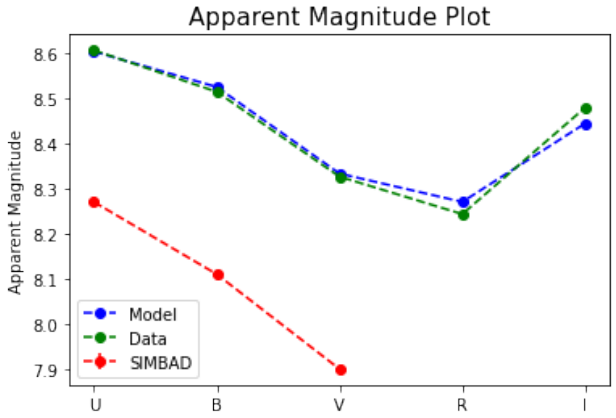

(f) HD 86986 (A1V star): Synthetic and observed apparent magnitude comparison

Figure 6.11: Horizontal Branch stars - relatively poor fit in U band along with high deviation of synthetic apparent magnitude values from observed values

In general, goodness of fit to giant stars is found to be variable, with the deviation in the photometric magnitudes ranging from 0.1 to 1. Here again, no particular correlation is found between the goodness of fit in flux distribution (as observed from residual values) and the fit in apparent magnitude in various bands. Further, no general trend can be inferred from the set of sample sources considered, partly due to low sample size (see Figure 6.14). The range of residuals is the similar to that observed in main sequence stars.

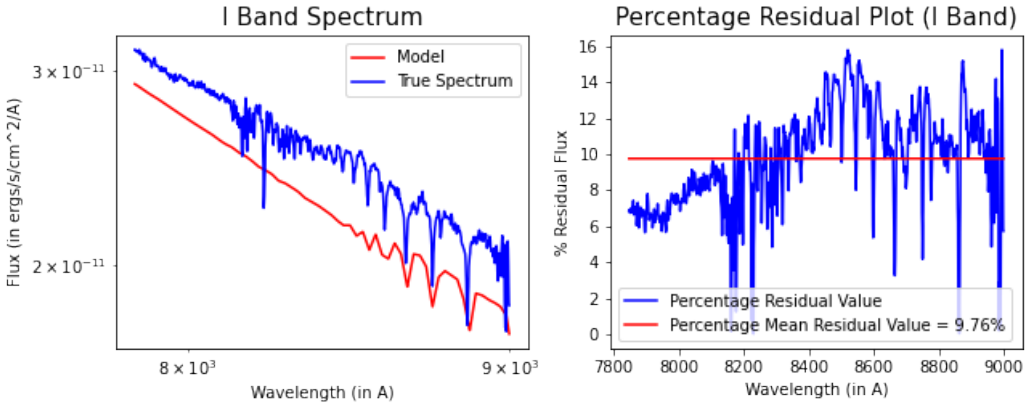

(a) HD 91316 (B1Ib star)

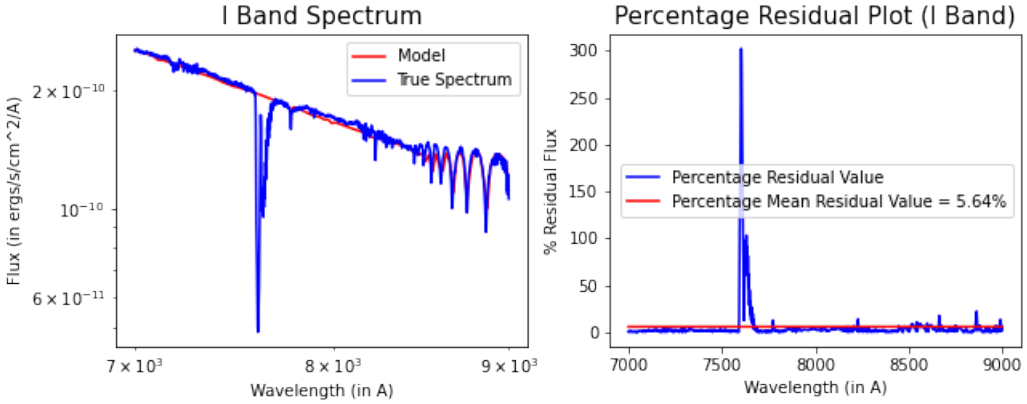

(b) HD 95418 (AIV star)

Figure 6.12: Paschen series well fit by synthetic SED in B-A stars

In the sample of stars considered, good fit in flux distribution along with good match in apparent magnitude (deviation $\sim 0.2-0.3$) is observed in A,B and G type sub-giants (see Figure 6.14). Most of the sub-giant stars in the original dataset were found to be either double stars or spectroscopic binaries, due to which, they were ignored from analysis, leading to low number of sub-giant sources in the sample set considered.

The photometric magnitude values obtained from Kurucz model synthetic flux distribution is found to not match well the values given in J.-F.

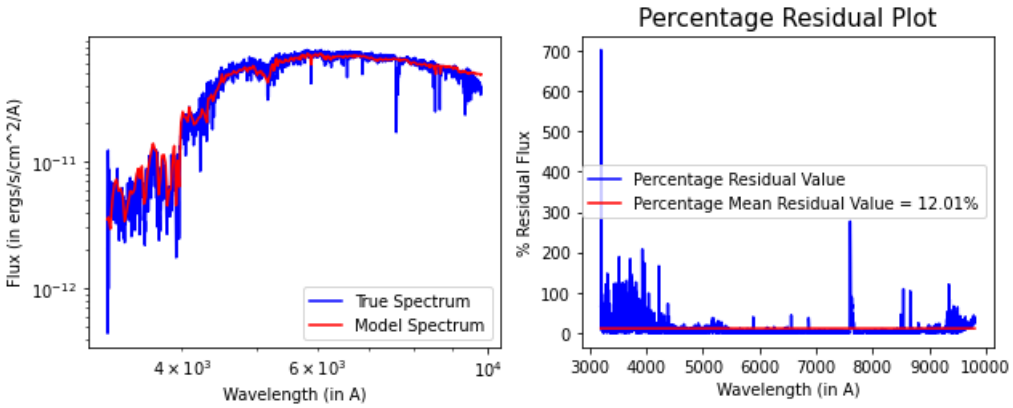

(a) HD 94247 (K3III star)

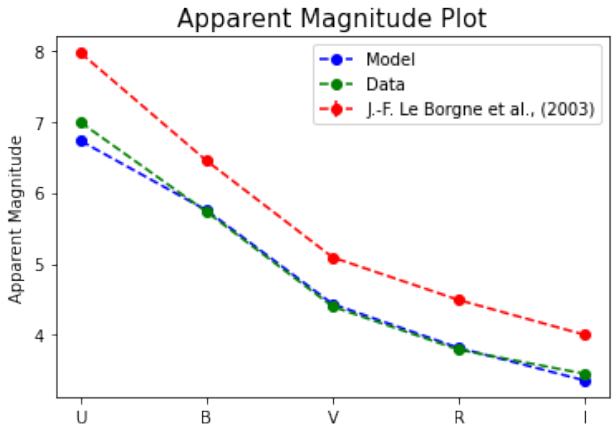

(b) HD 94247 (K3III star): Synthetic and observed apparent magnitude comparison

Figure 6.13: Giant stars - no general trend observed regarding goodness of fit among different spectral types of stars

Le Borgne et al. (2003) and SIMBAD database. For most of the stars considered, the photometric flux values are found to deviate by about 0.5 magnitudes (in some cases, by 1.0 magnitude) around the observed value (some with very little deviation or spread and some with very high). One of the possible reason (partially) could be difference in the filter transmission curves used for synthetic photometry and observational photometry.

Here again, we observe significant spread in the observed magnitudes of

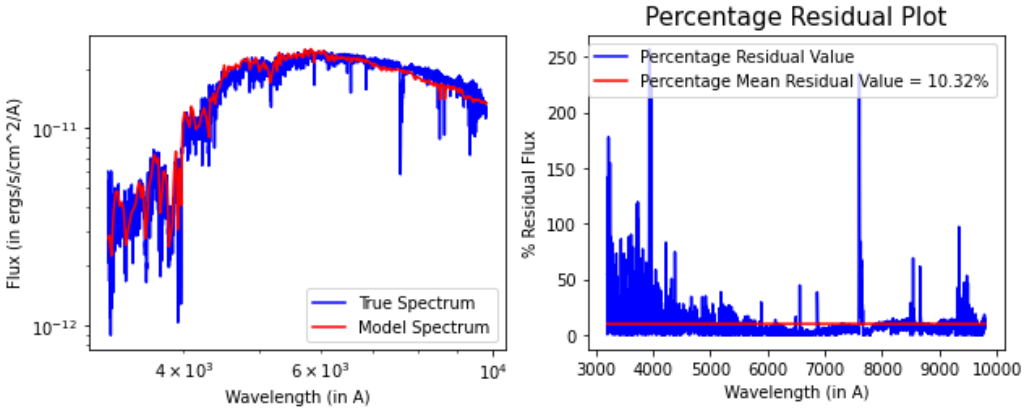

(c) HD 100006 (K0III star)

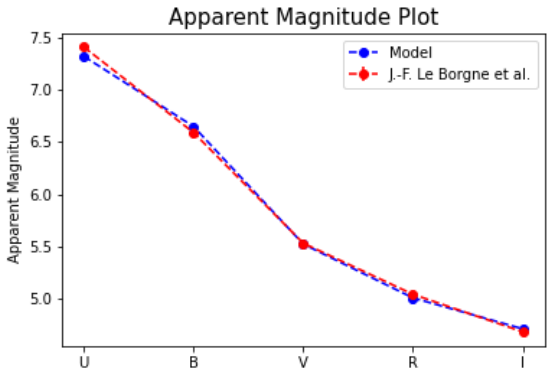

(d) HD 100006 (K0III star): Synthetic and observed apparent magnitude comparison

Figure 6.13: Giant stars - no general trend observed regarding goodness of fit among different spectral types of stars

the stars of each spectral type, which indicates that the selection effects are minimized.

Effect of T_{eff}, log(g), [Fe/H] on model SED

:

1. T_{eff}: We observe an increase in the overall flux with increase in effective

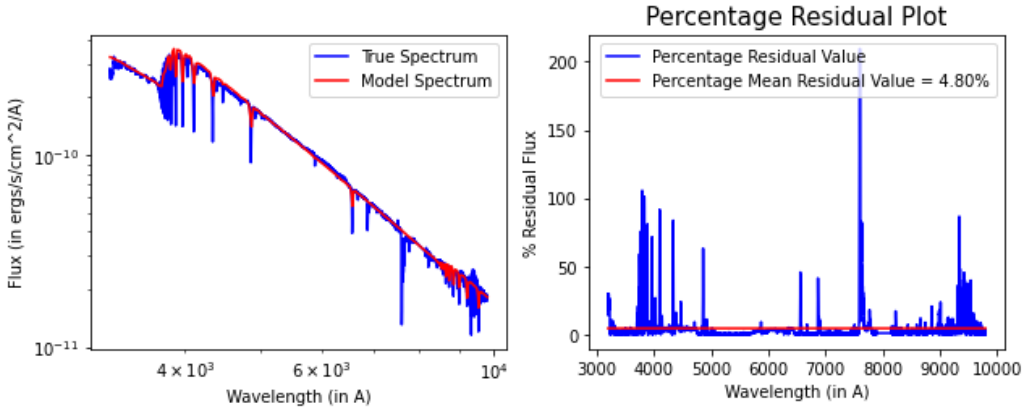

(a) HD 147394 (B5IV star)

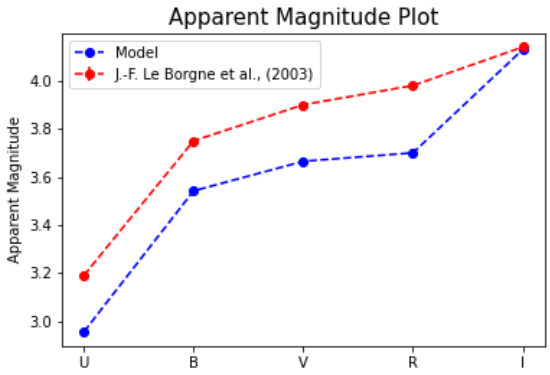

(b) HD 147394 (B5IV star): Synthetic and observed apparent magnitude comparison

Figure 6.14: Giant stars - no general trend observed regarding goodness of fit among different spectral types of stars

temperature

2. log(g): Variation of the value of log(g) between lowest to highest possible values, we observe that the flux in the U band for wavelength range below Balmer limit increases whereas the same decreases in the B and V bands with no significant variation in the flux in R and I bands. No visible variation is seen (in terms of fit) due to variation (about the optimal values) - observable though the variation in metrics (such as mean residual value, chi-square value, etc.,).

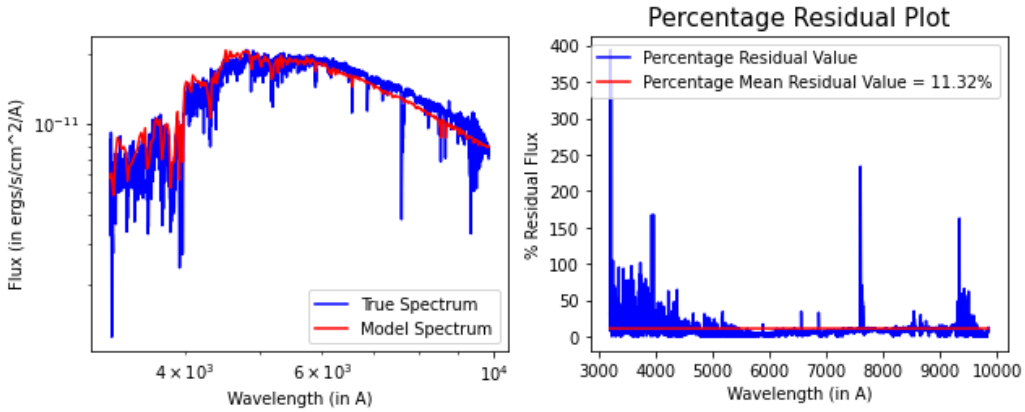

(c) HD 67767 (G8IV star)

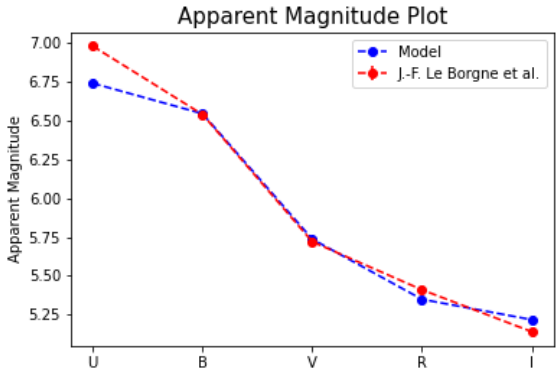

(d) HD 67767 (G8IV star): Synthetic and observed apparent magnitude comparison

Figure 6.14: Subgiant stars - poor fit for G type subgiant stars and good fit for B type subgiants

Fe/H : With increase in metallicity values, we observe that the model SED is able to fit the Calcium K line ($\approx$ 3968A), in the U band. Also, we observe an overall increase in the flux in longer wavelength range (R and I bands).

6.1.1 Separate B and V Band Fit Analysis

From the plot of parameters derived from fitting Kurucz models (using the procedure described above, with the search restricted to values of around the values published for each source) to only the B or V band spectrum and that published, we make the following observations and inferences:

1. T_{eff}: We observe that very few sources have model spectrum fit with T_{eff} value differing by 100K. Thus, inferring that with some estimate of the effective temperature, one can obtain (using grid search around the same) a model spectrum that best matches the observed spectrum with low residuals.

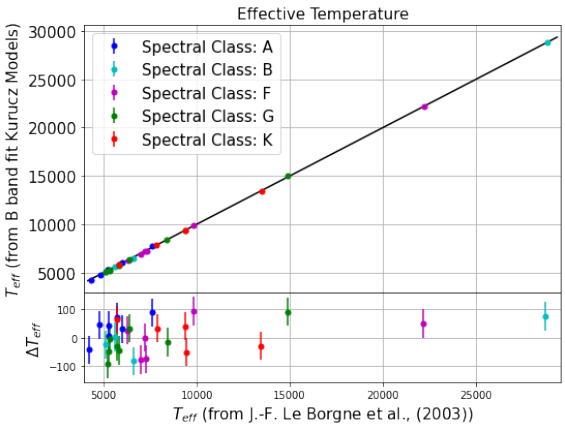

(a) T_{eff} value from B Band fit compared to that published

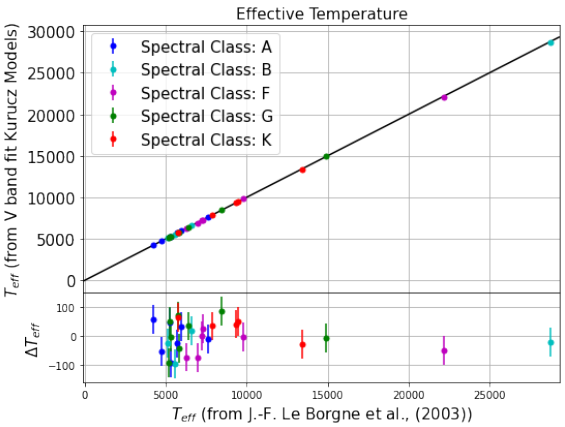

(b) T_{eff} value from V Band fit compared to that published

2. $log(g)$: We observe that most of the sources have model spectrum fit with $log(g)$ value differing by less than 0.15 dex. Thus, inferring that with some prior estimate of the surface gravity or with knowledge of the type of star (hence, restraining the search for the values within the range), one can obtain a model spectrum that best matches the observed spectrum.

3. $[Fe/H]$: We observe that very few sources have model spectrum fit with metallicity value that differs from published values by a values greater than 0.10 dex. Thus, inferring that with some prior estimate of

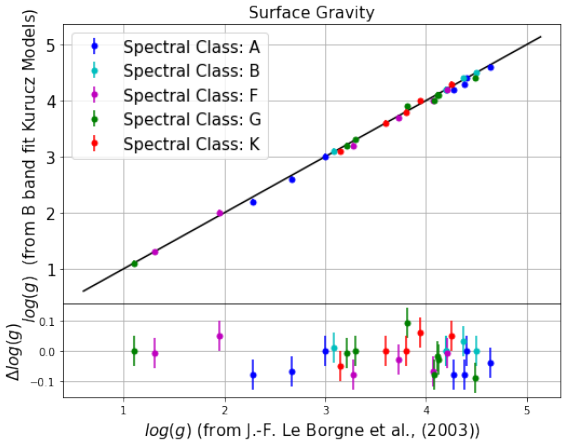

(a) $log(g)$ value from B Band fit compared to that published

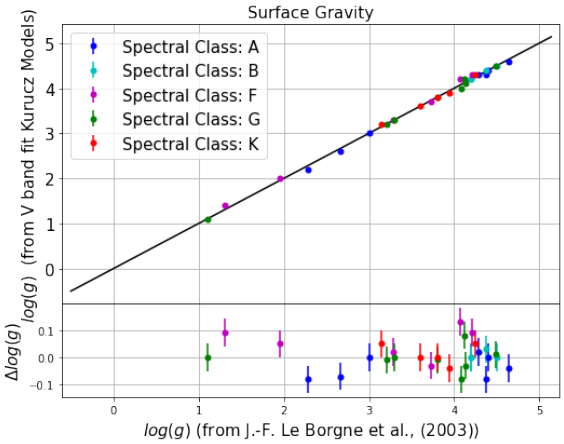

(b) $log(g)$ value from V Band fit compared to that published

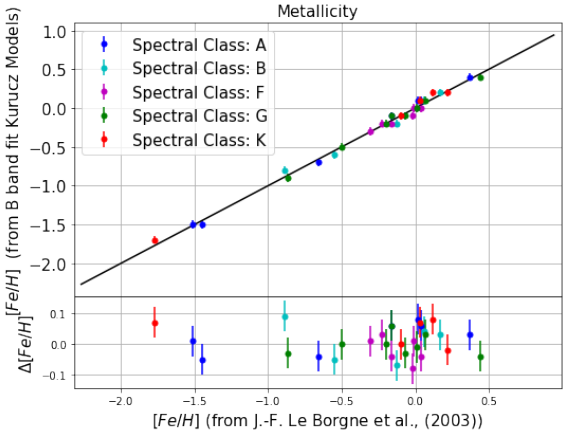

(a) $[Fe/H]$ value from B Band fit compared to that published

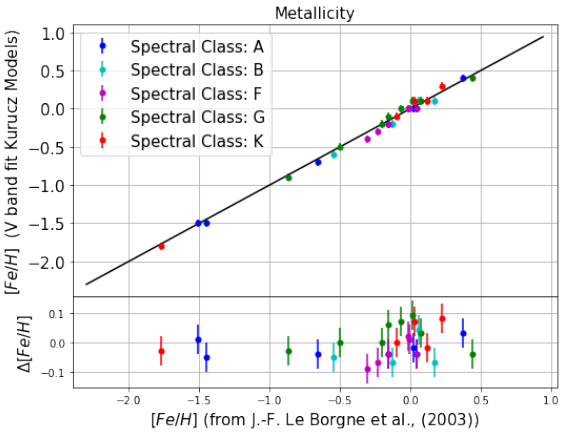

(b) $[Fe/H]$ value from V Band fit compared to that published

the metallicity (by determining the same by other methods), one can obtain a model spectrum that best matches the observed spectrum.

All model spectrum were obtained to have a mean residual values much less than 10%.

From the plot of parameters derived from fitting Kurucz models (using the procedure described above) to only the B or V band spectrum and that

to the complete spectrum available, we make the following observations and inferences:

1. T_{eff}: We observe that very few sources have model spectrum fit with T_{eff} value differing by 100K. Thus, we infer that the effective temperature derived from the fit of model spectrum to the complete available flux distribution and that to only the B or V band spectrum, matches well with the deviation of the order of half the span of the range explored (with the center value of the range obtained from an estimate of the effective temperature).

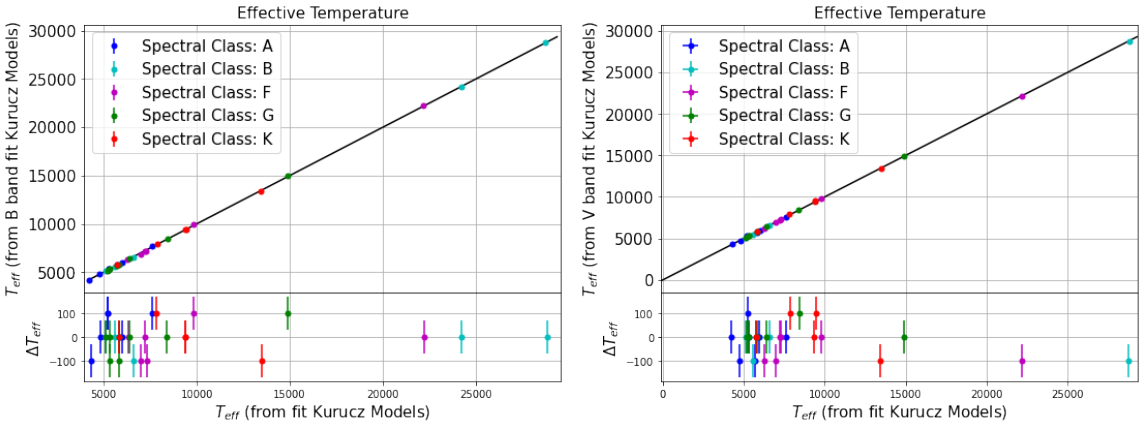

(a) T_{eff} value from B Band fit compared to that of fit to complete available flux distribution

(b) T_{eff} value from V Band fit compared to that of fit to complete available flux distribution

2. $log(g)$: We observe that very few sources have model spectrum fit with $log(g)$ value differing by 0.1 dex. Thus, we infer that the surface gravity derived from the fit of model spectrum to the complete available flux distribution and that to only the B or V band spectrum, matches well with the deviation of the order of half the span of the range explored (with the range obtained from knowledge of the type of star).

3. $[Fe/H]$: We observe that very few sources have model spectrum fit with metallicity value differing by 0.1 dex. Thus, we infer that the effective temperature derived from the fit of model spectrum to the complete available flux distribution and that to only the B or V band

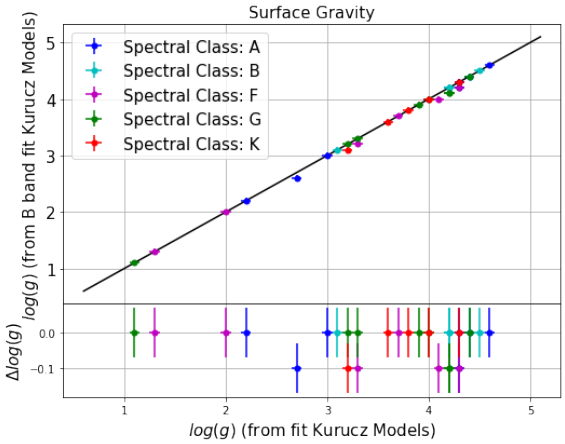

(a) $log(g)$ value from B Band fit compared to that of fit to complete available flux distribution

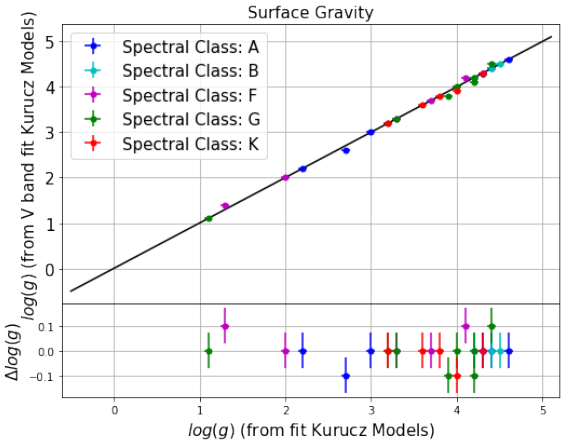

(b) $log(g)$ value from V Band fit compared to that of fit to complete available flux distribution

spectrum, matches well with the deviation of the order of half the span of the range explored (with the center value of the range obtained from an estimate of the metallicity by other independent methods).

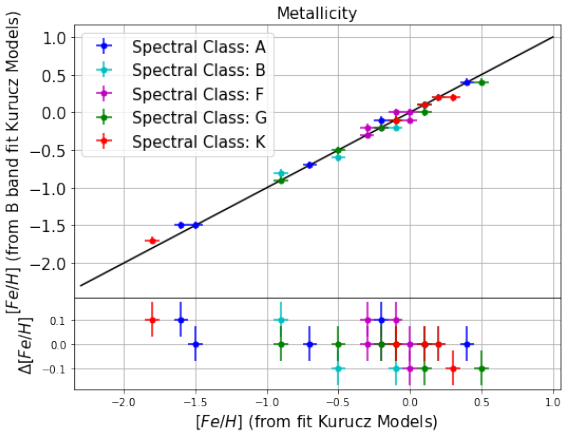

(a) $[Fe/H]$ value from B Band fit compared to that of fit to complete available flux distribution

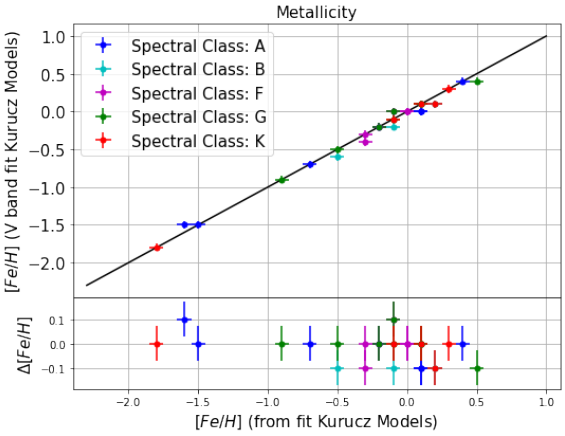

(b) $[Fe/H]$ value from V Band fit compared to that of fit to complete available flux distribution

4. $R/R_{\odot}$: We observe that very few sources have model spectrum fit with $R/R_{\odot}$ value differing a value greater than 10. Thus, we infer that

the radius of the star derived from the fit of model spectrum to the complete available flux distribution and that to only the B or V band spectrum, matches well for small sized stars, though the deviation (and the error/uncertainty) increases with increase in the size of the source. Hence, reliable estimates can be obtained only for main-sequence and subgiant stars (with deviation < 2). For giant stars, the deviation increases ($10R_{\odot}$), hence, only an estimate can be obtained, not any reliable value.

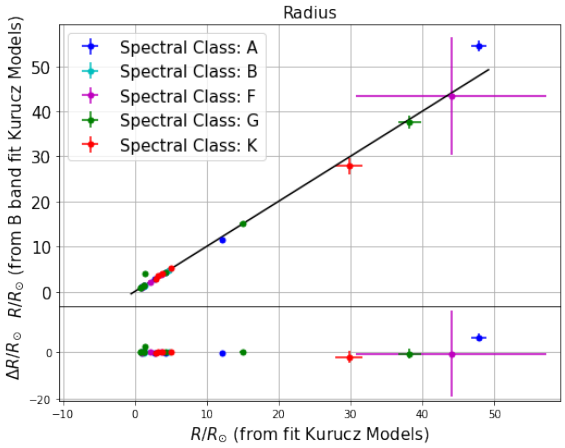

(a) $R/R_{\odot}$ value from B Band fit compared to that of fit to complete available flux distribution

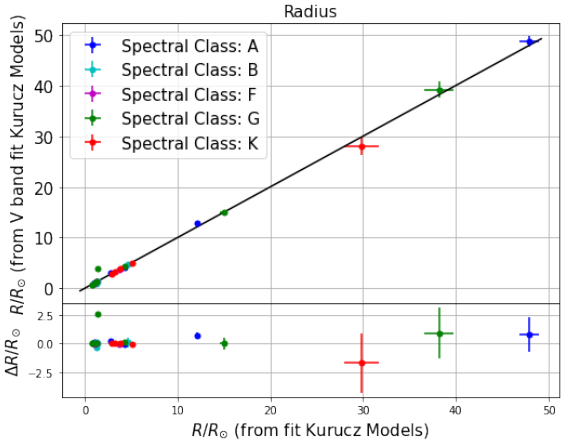

(b) $R/R_{\odot}$ value from V Band fit compared to that of fit to complete available flux distribution

From the plot of apparent magnitudes (B and V) and color (B-V) values published to that derived by fitting Kurucz models to only the B and only V band spectrum and that to the complete spectrum available, we make the following observations and inferences:

1. Apparent magnitudes: We observe that for most of the sources V band magnitudes is predicted by the model to be lower than that published (i.e., predicted to be brighter than observed values). In case of B band magnitude, most of the stars have a value within 0.2 dex of the published value. For few sources, the deviation is observed to be of the order of 0.4 dex with few outliers having a value exceeding 0.4 dex. For most of the stars having a difference greater then 0.4 dex have been predicted to be brighter than observed, with the difference ≤ 1 dex.

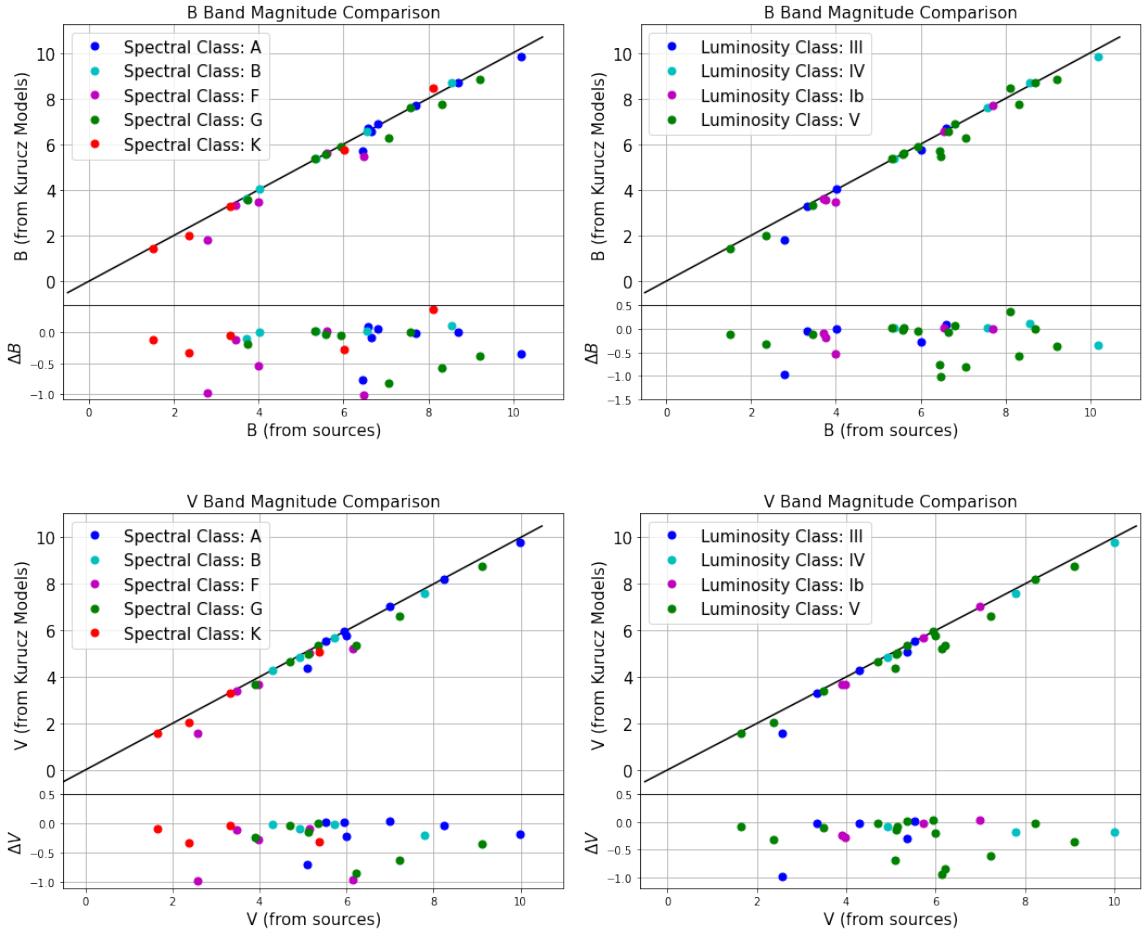

Figure 6.22: Apparent magnitude from fit only to specific bands compared to that published.

2. Colors: We observe that the deviation of the B-V color values from the observed value is less than 0.2 dex (with very few outliers). Thus, we infer that the color derived from the fit of model spectrum to only the B and only V band spectrum, matches well with the observationally obtained values, with the deviation of the order of few tenths of dex.

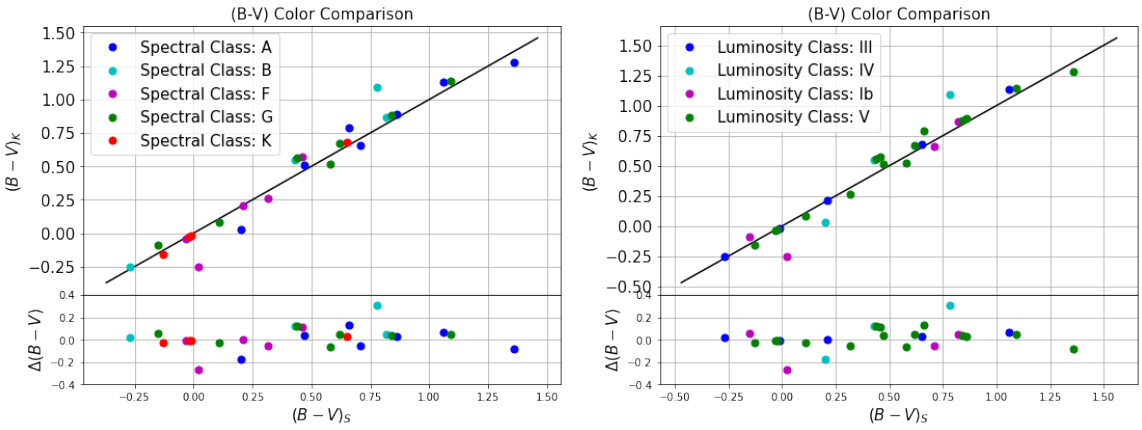

Figure 6.23: (B-V) value from B and V Band fit compared to that published

From the plot of apparent magnitudes (B and V) and color (B-V) derived from fitting Kurucz models (using the procedure described above) to only the B or V band spectrum and that to the complete spectrum available, we make the following observations and inferences:

1. Apparent magnitudes: From Figure 6.24, we observe that very few sources have B and V band apparent magnitudes differing by a value greater than 0.2 dex from that obtained by fitting model spectrum to the complete available flux distribution. Thus, overall we infer that the apparent magnitudes derived from the fit of model spectrum to the complete available flux distribution and that to only the B or V band spectrum, matches well with the deviation of the order of few tenths of dex. Further, the deviation in V band magnitude for subgiants and giants is lower than that of main sequence stars.

2. Colors: From Figure 6.25, we observe that very few sources have B-V color values differing by a value exceeding 0.2 dex from that obtained by fitting model spectrum to the complete available flux distribution. Thus, we infer that the color derived from the fit of model spectrum to the complete available flux distribution and that to only the B and only V band spectrum, matches well with the deviation of the order of few tenths of dex. The sources are predicted to have a color value less than that determined from fit to the complete flux distribution for

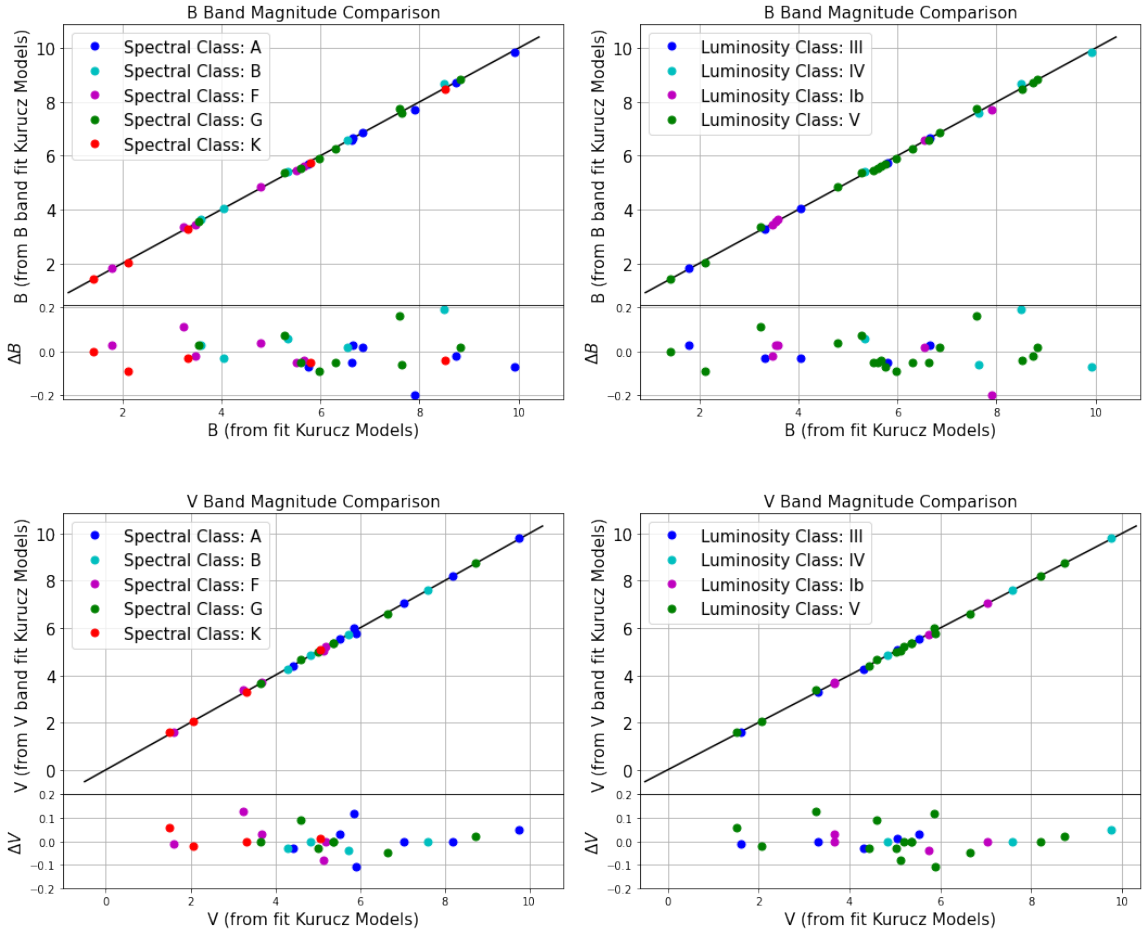

Figure 6.24: Apparent magnitude from fit only to specific bands compared to that determined from fit to the complete available flux distribution.

most of the stars.

It is observed that in spite of using filter transmission curves (for synthetic photometry) non-identical to those used in other sources (from which the observational photometric values are taken for comparison), the color values obtained from synthetic flux distribution matches well (with deviation ≤ 0.2 dex with observationally determined values. The effect of the non identicalness of the filter transmission curves if more pronounced in the apparent magnitudes determined synthetically, which is the plausible reason

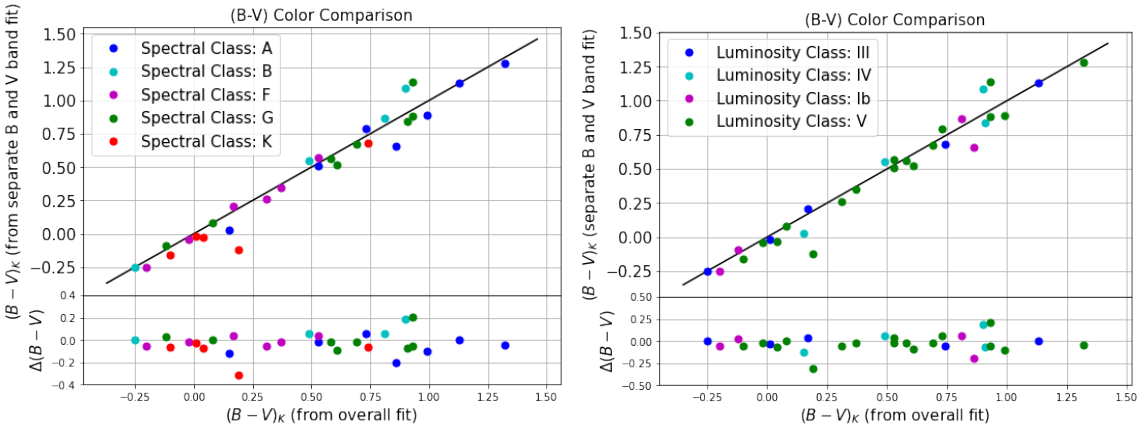

Figure 6.25: (B-V) value from B and V Band fit compared to that determined from fit to complete available flux distribution

for the deviations of the order of 1 dex.

Further, the fit parameter values determined from fit only to B and V bands of flux distribution are compared. We observe that high variation is observed between fit value of effective temperature in B and V bands in stars with temperature less than 10000K. On contrary, the deviation is low in case of surface gravity is low in most sources. In case of metallicity, the amount of spread in the values is higher in stars predicted with solar metallicity, though the degree of agreement between the same is high in metal rich stars. High variability in values of fit parameters is observed in case of main sequence stars, relative to other type of stars.

6.2 IRTF Data Analysis

The dataset that has been taken for the analysis is retrieved from NASA InfraRed Telescope Facility Archive[55]. Minimum of 4 sources belonging to each of the three spectral classes (F, G, and K) in the dataset, for which the fit parameters values were available from publications from various authors have been selected for analysis. Sources which are isolated stars are considered, ignoring binary stars or double stars from analysis. The results of the analysis is presented in this section. Pictorial representation of various results obtained is presented for enhanced clarity.

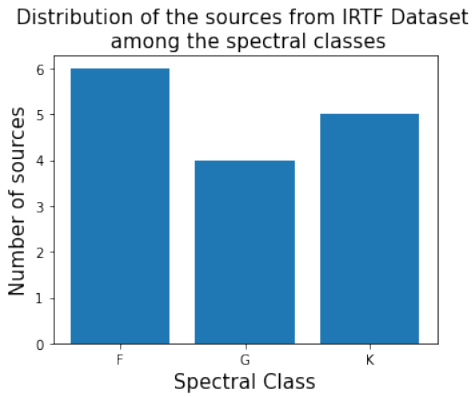

Figure 6.26: Number of sources in considered data subset per spectral class

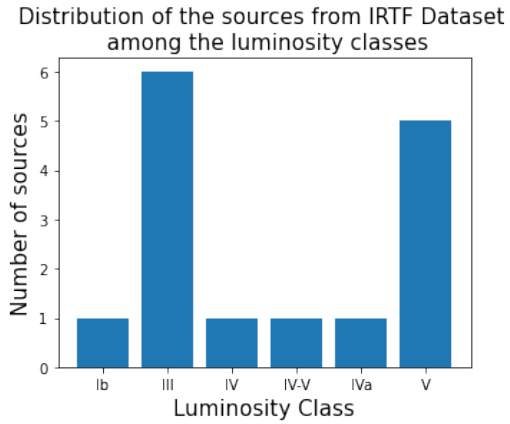

Figure 6.27: Number of sources in considered data subset per luminosity class

Table 6.3 contains the information regarding the values of the fit parameters obtained by fitting Kurucz model spectral energy density with observed flux data and the same as obtained from research papers. The name of the source (as in Henry Draper Catalogue) and their spectral type (as given in the NASA IRTF archive[55] from which data was retrieved for analysis) is also mentioned.

Throughout the analysis, the step size of effective temperature of the fit was limited to 100K, surface gravity and metallicity to 0.1 dex and radius (expressed in terms of faction of radius of sun) to first decimal place.

The Figures 6.28, 6.29 and 6.30 represents a comparison between fit and

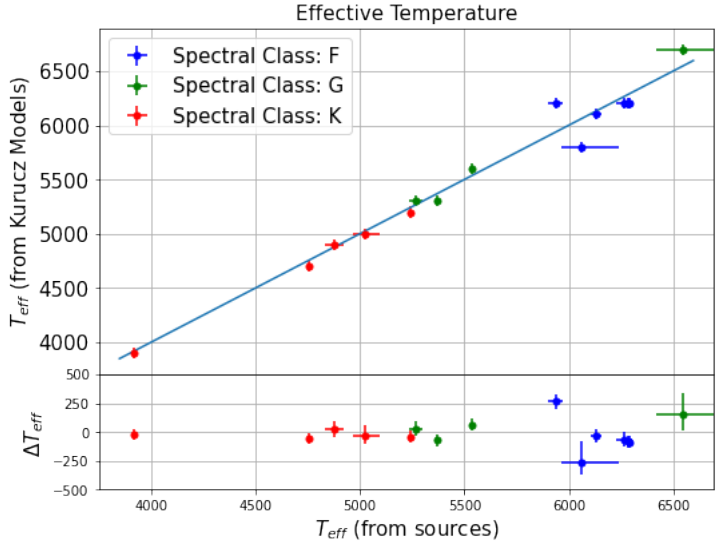

Figure 6.28: Comparison between fit and published values of T_{eff}

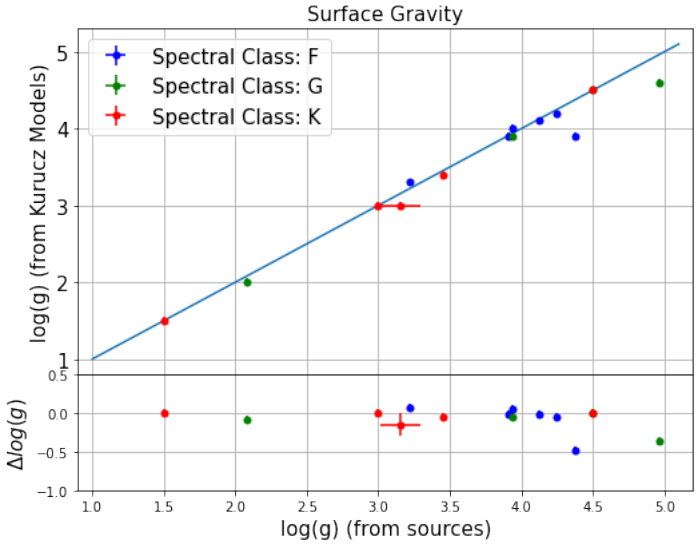

Figure 6.29: Comparison between fit and published values of $log(g)$

published values of three parameters being fit, namely, effective temperature (T_{eff}), surface gravity (log(g)), metallicity ([Fe/H]).

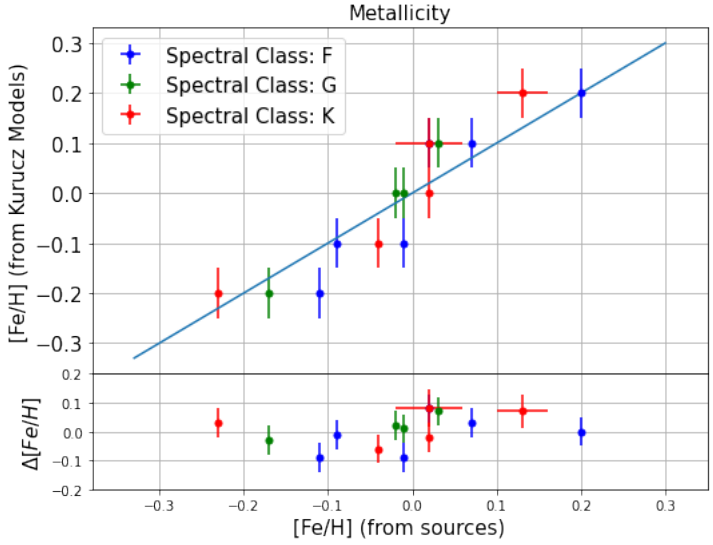

Figure 6.30: Comparison between fit and published values of $[Fe/H]$

We observe from the comparison plot of effective temperature that the effective temperature predicted by Kurucz models is lower than that of published value in most of the cases. The deviation from the published values of effective temperature is least for K type stars and most for F type stars.

In the comparison plot of surface gravity, we observe that the value predicted by Kurucz models is lower than that of published value for most of the stars in the dataset considered.

In the comparison plot of metallicity, we observe step variation in the predicted values of the same with respect to the published values. For all values of metallicity between -0.25 and -0.1 dex, value predicted by Kurucz models is -0.2, sources with published values of metallicity between -0.1 and 0.0 (or approximately, 0.05) are predicted to have solar metallicity. Similar trend is observed for metal-poor (metal-weak) stars.

Further, all the F-type stars are predicted to be either metal-rich or metal-poor. Most of the G-type stars with close to solar metallicity are predicted to have solar metallicity (partly, due to limitation on the grid search precision) and those metal-poor or metal-rich are predicted to be so. The

spread in metallicity predicted by Kurucz models for K-type stars (sources) with similar (difference less than $\sim$0.05 dex) values of metallicity is found to be high. As can be seen from the plot, out of two K-type stars with metallicity close to solar value ($0.0 < [Fe/H] < 0.05$), one is predicted to have solar metallicity and other to be metal-poor. One with $-0.05 < [Fe/H] < 0.0$ is qualitatively predicted to be metal-poor ($[Fe/H] = -0.1$). Thus, when searched for metallicity values around the value determined by other independent method (for example, Equivalent-Width Method), we will be able to obtain physically acceptable predictions (which match qualitatively) without much compromise in the goodness of fit. It was observed that letting the metallicity as a free parameter leads to Kurucz models with physically unacceptable metallicities (usually offset from the independently determined value by about 0.3 dex). Thus, to overcome this issue, it is found to be necessary to determine the metallicity by other methods.

The photometric magnitude values obtained from Kurucz model synthetic flux distribution is found to be within the error bars of the values from 2MASS data. For most of the stars considered, the photometric flux values are found to be close to the mean value with very few stars' synthetic photometry just crossing the error bars. Thus, we can infer that the synthetic flux distribution from Kurucz models, when well fit to the observed flux distribution, can be used to infer the photometric properties of the star, with high accuracy. The deviation of synthetically determined photometric magnitudes from that determined observationally are observed to be of first order (mismatch mostly in first decimal), with some having mismatch only in second decimal (i.e., good match).

The synthetic photometry of K-type stars are found to match with the observational photometry. Some mismatch is found in F- and G-type stars.

A trend is observed in the synthetic photometry using Kurucz models, where in cases of high mismatch between J and H band magnitude, a low mismatch between Ks band magnitude is observed and vice-versa. (as shown in the Figure 6.32 and 6.33). No mismatch between synthetic and observed photometry in K-type stars may be due to selection effects. Hence, no general inference regarding K-type star. Yet, in general a good match between synthetic and observed photometric magnitudes is in the infrared wavebands (J, H and Ks, as considered here).

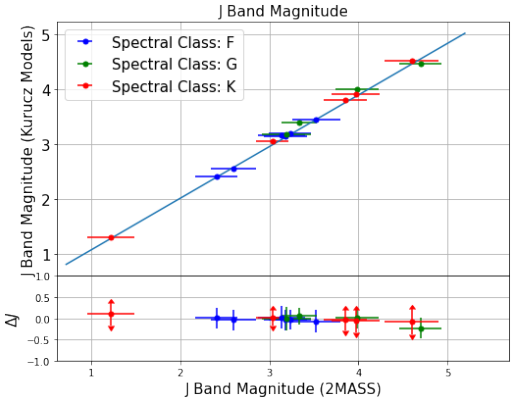

(a) J Band Magnitude Comparison

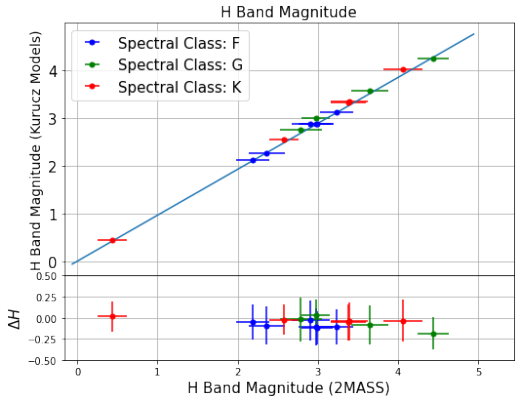

(b) H Band Magnitude Comparison

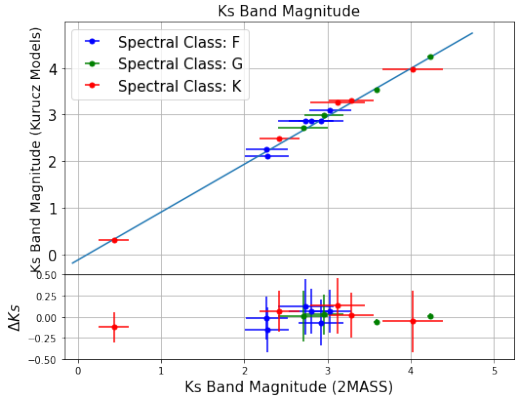

(c) Ks Band Magnitude Comparison

Figure 6.31: Comparison between synthetic photometric values and observational values (from 2MASS database)

The fit of the model flux distribution to the observed with mean residual value being less than 10%. Most of the stars' observed flux distribution in the considered wavelength range (0.8-5.0μm) are fit by Kurucz model flux distribution with a mean residual values $\sim 2-3\%$ (with high residual values in some exceptional cases). In some stars, it is observed that the fit is not good in particular wavebands, though the fit is good overall or in other wavebands. Also, in some cases it is found that the model flux is either greater or lesser than the observed flux distribution through out a particular waveband. These cases are due to limited precision of search for radius parameter

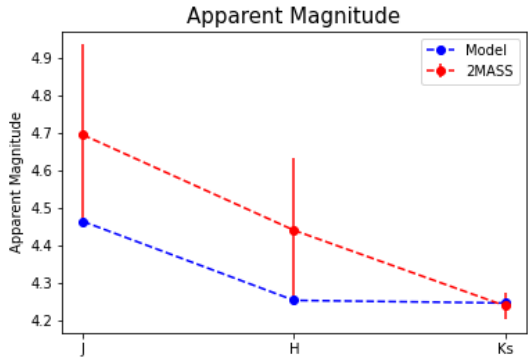

Figure 6.32: HD 21770: G-type Star - High mismatch in J and H band magnitude, though good match in Ks band magnitude

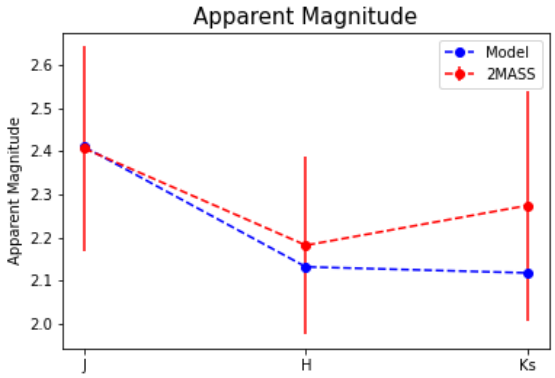

Figure 6.33: HD 11443: F-type Star - High mismatch in Ks band magnitude, though within (very high value) error bar

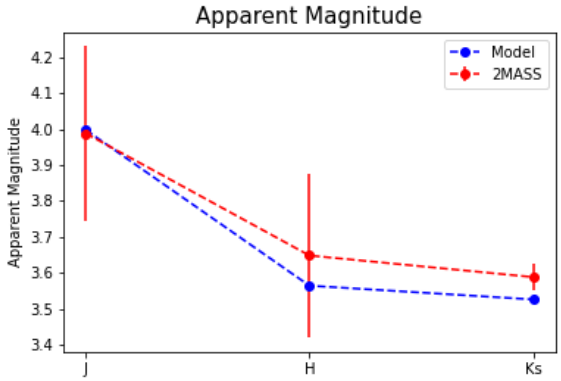

Figure 6.34: HD 101501: G-type Star - Ks band magnitude not within (very low value) error bar

value ($0.1R_{\odot}$), which can be resolved by scaling (which, essentially is increasing the search to second or higher decimal places).

Similarly, high mismatch is observed in J and H bands fit for HD 115617 (G-type star), with a good match in Ks band. Maximum mean residual value ($\approx 9.556\%$ over the whole wavelength range considered) is observed for the source HD 114710 (F-type star).

```
Best fit model parameters:
Log(g) = 4.6 [0.05]
Teff = 5300 [50]
[Fe/H] = log_10((Fe/H)star/(Fe/H)sun) = 0.1 [0.05]
R = 0.9 [0.05] R_sun
Md = 4.4869275653912874e-18
Chi-square value = 1232.6402509361003
p value = 1.0
Percentage Mean Residual Value = 5.726354100000756 %

<matplotlib.legend.Legend at 0x7fabc347f438>
```

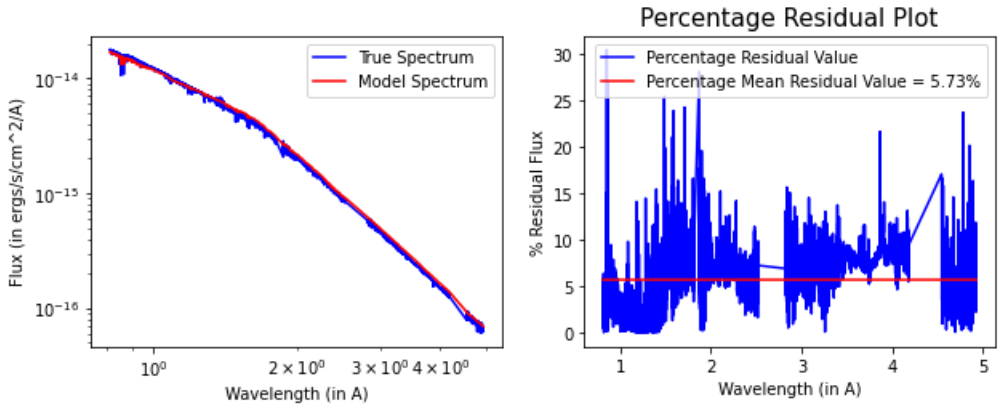

Figure 6.35: HD 101501: G-type star - example of mismatch in flux distribution in specific wavebands

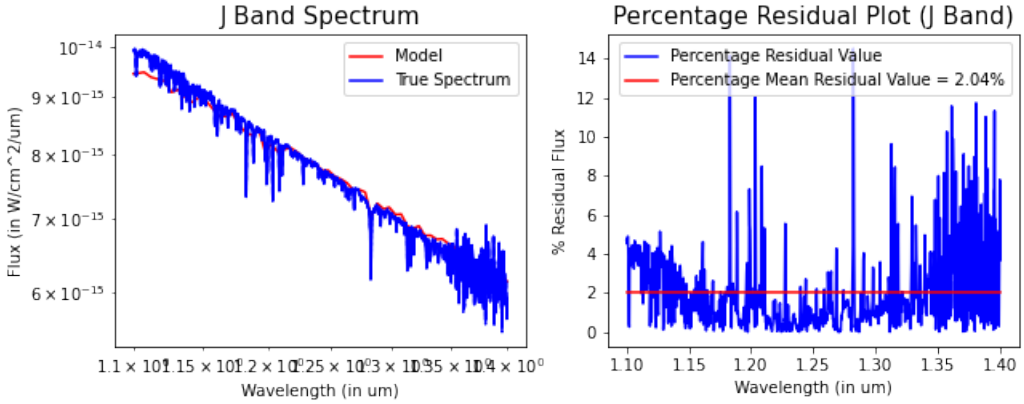

Figure 6.36: HD 101501: G-type star - good match between model and observed flux distribution in J band

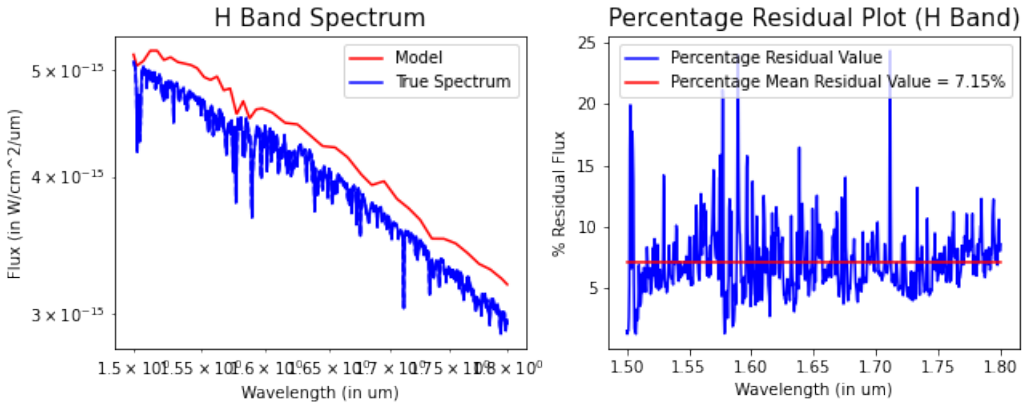

Figure 6.37: HD 101501: G-type star High mismatch in H band flux distribution

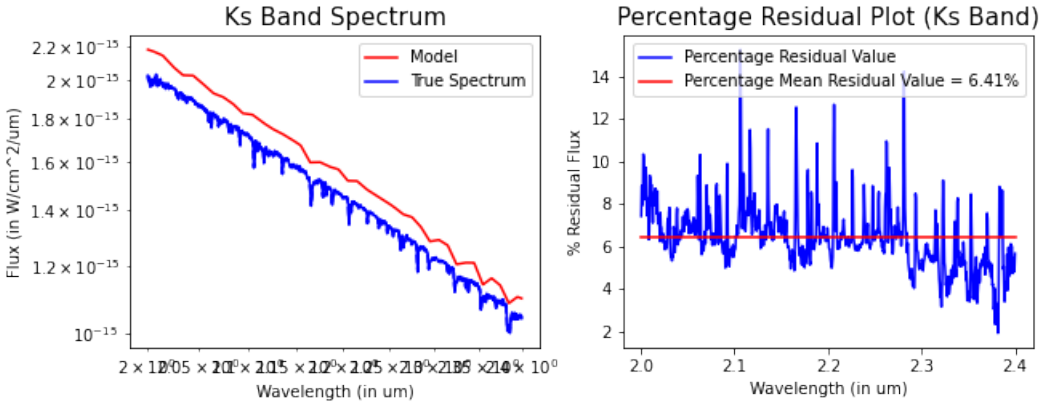

Figure 6.38: HD 101501: G-type star High mismatch in Ks band flux distribution

Another prominent features observed in Kurucz model flux distribution is that the spectral lines are fit by the model with high accuracy. The equivalent width of the model and observed spectral lines do not match precisely, though the wavelength of spectral line is matched with high precision. (see Figure: 6.11 through 6.13)

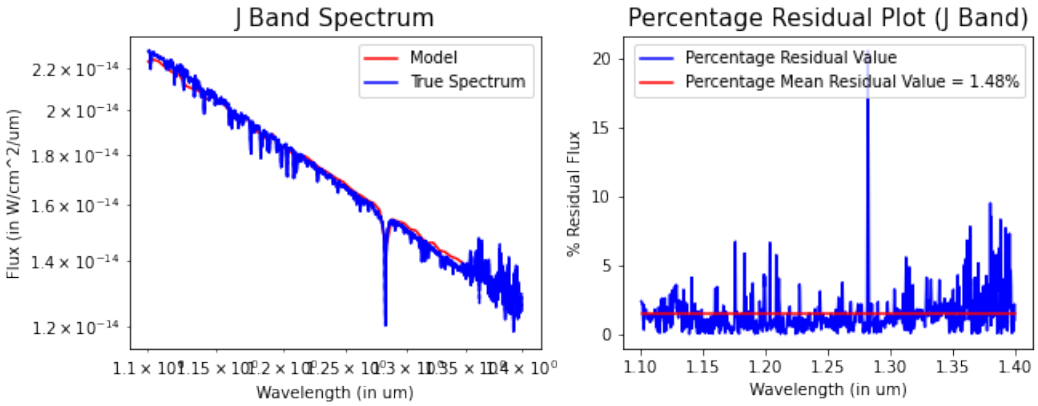

Figure 6.39: HD 126660: F-type Star - an example of Paschen (n:3-5) series line at $\approx 1.28\mu m$ well fit by Kurucz model flux distribution, in the J band

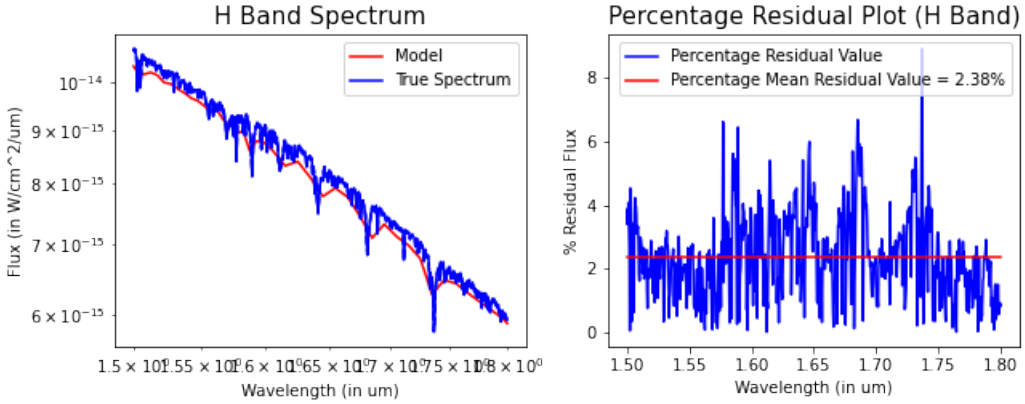

Figure 6.40: HD 124850: F-type Star - an example of coincidence of wavelengths of spectral lines in model and observed flux distribution, in H band

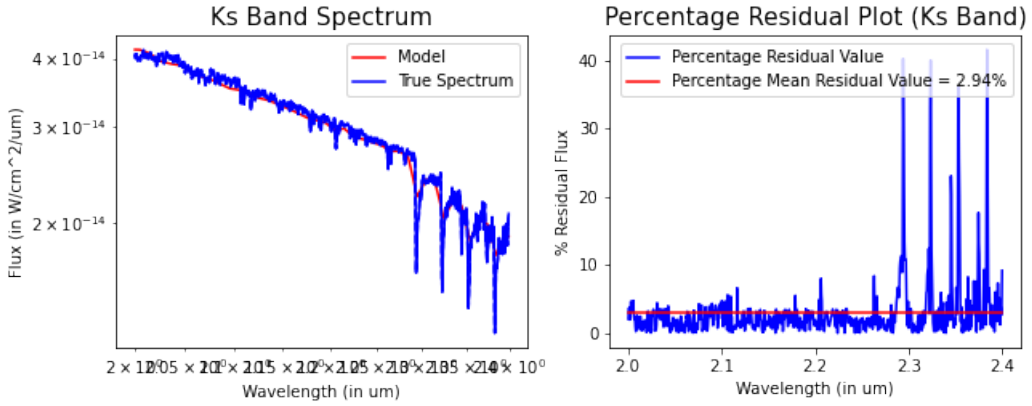

Figure 6.41: HD 120477: K-type Star - example of spectral lines in observed flux distribution well fit by Kurucz model flux distribution (in Ks band)

Thus, we can infer that in general, the Kurucz models can be used to obtain synthetic spectral energy distribution that best matches the observed flux distribution in the infrared wavelength range.

In cases where the temperature (by two-color method), radius (by interferometric or occultation methods), metallicity (by equivalent width or alike method) and surface gravity (a range can be obtained using radius or with the knowledge of the type of star) are available (with no spectrum available for direct determination of metallicity), a reliable estimate of the photometric magnitude values in the infrared wavelength range can be obtained.

Chapter 7

Conclusion

From the analysis performed, we conclude that Kurucz models are suitable for application in fitting main sequence stars. No Kurucz models are available for hypergiant stars. The goodness of fit deteriorates from main sequence to giant stars. Horizontal branch stars are well fit by Kurucz models, mainly in BVRI bands though it does not fit all the lines in Balmer series visible in the U band due to low resolution of the synthetic SED, despite which significant mismatch is observed in synthetic photometry of horizontal branch star. One can obtain the best fit model with physically acceptable (which also matches with that determined independently by other methods) parameter values for effective temperature and surface gravity by constraining the region of grid search to appropriate range. Even in case of availability of estimate of range of possible values of metallicity, it is not advocated to use Kurucz models to search for best metallicity for the star, unless the span of grid search range is small ($\sim$ 0.1dex).

Chapter 8

Future Scope

With most of the analysis restricted to use of prior knowledge of the grid search parameters and only explored the goodness of fit of flux distribution and match between synthetic photometry and that observed, we hope to extend the work to determine the grid search parameters, not accurately obtained from grid search of Kurucz models, mainly the metallicity values. Also, we intend to determine the range of possible values of effective temperature and surface gravity for restricting the grid search, to obtain both good fit for flux distribution and also obtain accurate values of the same parameters. New and larger datasets can be used for the analysis to analyse the results statistically, as the number of sources belonging to each spectral or luminosity class in the presently used data sub-set is too low for use in any statistical inferences (like, statistical determination of goodness of match between synthetic and observed photometry, tests to determine whether each of the types of spectral and luminosity classes are well fit by Kurucz models or not, statistical determination of absence of any selection effects/biases in the type of stars). Spline or local (3-point) Lagrange interpolation can be used in place of linear interpolation to obtain smoother model flux distributions. Further, the analysis can be extended to the analysis of other stellar atmosphere models such as MARCS, Phoenix, BaSTI models, and many more, and compare and contrast each model (to determine which model is suitable for which particular class or type of stars).

Appendix A

Results

A.1 STELIB Dataset Results

A.1.1 Results for Fit over complete SED

Star	**Spectral Type**	Best Fit Parameter Values				Published Parameter Values			
		T_{eff} (K)	log(g) (dex)	[Fe/H] (dex)	$R/R_{\odot}$	T_{eff} (K)	log(g) (dex)	[Fe/H] (dex)	$R/R_{\odot}$
HD 2857	A2IV[30]	7600 ± 50	2.7 ± 0.05	-1.6 ± 0.05	4.3 ± 0.19	7611	2.67	-1.51	-
HD 32537	F0V	7000 ± 50	4.1 ± 0.05	-0.3 ± 0.05	2.1 ± 0.05	6978	4.07	-0.23	1.56[41]
HD 34411	G0V	5800 ± 50	4.2 ± 0.05	0.1 ± 0.05	1.3 ± 0.05	5845	4.13	0.01	1.331 ± 0.021[5]
HD 34816	B0.5IV	28800 ± 50	4.2 ± 0.05	-0.1 ± 0.05	4.7 ± 0.29	28724	4.20	-0.13	-
HD 35497	B7III	13500 ± 50	3.8 ± 0.05	-0.1 ± 0.05	5.1 ± 0.07	13429	3.80	-0.10	4.2[47]
HD 36673	F0Ib	7300 ± 50	1.3 ± 0.05	0.0 ± 0.05	171.1 ± 16.2	7276	1.31	-0.02	-
HD 37394	K1V	5100 ± 50	4.2 ± 0.05	-0.2 ± 0.05	1.3 ± 0.07	5194	4.12	-0.20	4.2[47]
HD 39949	G2Ib	5300 ± 50	1.1 ± 0.05	-0.1 ± 0.05	38.2 ± 1.57	5250	1.10	-0.16	-

HD 41593	K0V	5300 ± 50	4.4 ± 0.05	0.1 ± 0.05	0.8 ± 0.05	5305	4.49	0.07	-
HD 50420	A9III	7200 ± 50	3.3 ± 0.05	0.0 ± 0.05	15.0 ± 0.39	7200	3.28	0.04	-
HD 60778	A1V	8400 ± 50	3.3 ± 0.05	-0.5 ± 0.05	3.6 ± 0.10	8416	3.30	-0.50	-
HD 61064	F6III	6400 ± 50	3.2 ± 0.05	0.5 ± 0.05	4.3 ± 0.05	6367	3.21	0.44	-
HD 63077	G0V	5800 ± 50	4.0 ± 0.05	-0.9 ± 0.05	1.2 ± 0.05	5731	4.08	-0.87	-
HD 65583	G8V	5200 ± 50	4.6 ± 0.05	-0.7 ± 0.05	0.8 ± 0.05	5295	4.64	-0.66	-
HD 67767	G8IV	5600 ± 50	4.4 ± 0.05	0.2 ± 0.05	2.8 ± 0.05	5598	4.37	0.17	-
HD 69897	F6V	6300 ± 50	4.3 ± 0.05	-0.3 ± 0.05	1.3 ± 0.05	6275	4.21	-0.31	1.3870 ± 0.0276[6]
HD 75732	G8V	5200 ± 50	4.3 ± 0.05	0.4 ± 0.05	1.0 ± 0.05	5256	4.38	0.37	0.960 ± 0.067 [24]
HD 76151	G3V	5800 ± 50	4.4 ± 0.05	0.1 ± 0.05	1.0 ± 0.05	5728	4.40	0.04	0.88[19]
HD 86728	G1V	5800 ± 50	4.3 ± 0.05	0.2 ± 0.05	1.3 ± 0.05	5737	4.25	0.12	1.247 ± 0.021[5]
HD 86986	A1V	7800 ± 50	3.2 ± 0.05	-1.8 ± 0.05	2.9 ± 0.07	7867	3.15	-1.77	-
HD 87737	A0Ib	9800 ± 50	2.0 ± 0.05	-0.1 ± 0.05	29.8 ± 1.86	9806	1.95	-0.01	47[40]
HD 91316	B1Ib	24200 ± 50	3.1 ± 0.05	-0.9 ± 0.05	44.0 ± 13.2	24200	3.09	-0.89	-
HD 94028	F4V	6000 ± 50	4.3 ± 0.05	-1.5 ± 0.05	1.0 ± 0.05	5969	4.28	-1.45	-
HD 94247	K3III	4300 ± 50	2.2 ± 0.05	-0.2 ± 0.05	47.9 ± 1.04	4243	2.28	-0.16	-
HD 95418	A1V	9400 ± 50	4.0 ± 0.05	0.3 ± 0.05	3.3 ± 0.05	9452	3.94	0.22	-
HD 97633	A2V	9400 ± 50	3.6 ± 0.05	0.1 ± 0.05	3.9 ± 0.05	9360	3.60	0.03	-

HD 100006	K0III	4800 ± 50	3.0 ± 0.05	0.1 ± 0.05	12.1 ± 0.18	4755	3.00	0.02	-
HD 132142	K1V	5100 ± 50	4.5 ± 0.05	-0.5 ± 0.05	0.9 ± 0.05	5125	4.50	-0.55	-
HD 134083	F5V	6600 ± 50	4.2 ± 0.05	0.1 ± 0.05	1.4 ± 0.05	6583	4.20	0.06	-
HD 147394	B5IV	14900 ± 50	3.9 ± 0.05	-0.1 ± 0.05	4 ± 0.05	14908	3.81	-0.07	-
HD 164353	B5Ib	22200 ± 50	3.7 ± 0.05	-0.2 ± 0.05	17.2 ± 4.83	22150	3.73	-0.16	-

Table A.1: STELIB Dataset: Comparison of Parameter values from Kurucz Models with published values

A.1.2 Results for Fit over B-Band SED

Star	**Spectral Type**	Best Fit Parameter Values				Published Parameter Values			
		T_{eff} (K)	log(g) (dex)	[Fe/H] (dex)	$R/R_{\odot}$	T_{eff} (K)	log(g) (dex)	[Fe/H] (dex)	$R/R_{\odot}$
HD 2857	A2IV[30]	7700 ± 50	2.6 ± 0.05	-1.5 ± 0.05	4.2 ± 0.18	7611	2.67	-1.51	-
HD 32537	F0V	6900 ± 50	4.0 ± 0.05	-0.2 ± 0.05	2.1 ± 0.05	6978	4.07	-0.23	1.56[41]
HD 34411	G0V	5800 ± 50	4.1 ± 0.05	0.0 ± 0.05	1.3 ± 0.05	5845	4.13	0.01	1.331 ± 0.021[5]
HD 34816	B0.5IV	28800 ± 50	4.2 ± 0.05	-0.2 ± 0.05	4.8 ± 0.30	28724	4.20	-0.13	-
HD 35497	B7III	13400 ± 50	3.8 ± 0.05	-0.1 ± 0.05	5.1 ± 0.07	13429	3.80	-0.10	4.2[47]
HD 36673	F0Ib	7200 ± 50	1.3 ± 0.05	-0.1 ± 0.05	171.0 ± 16.29	7276	1.31	-0.02	-
HD 37394	K1V	5100 ± 50	4.1 ± 0.05	-0.2 ± 0.05	1.3 ± 0.05	5194	4.12	-0.20	4.2[47]
HD 39949	G2Ib	5200 ± 50	1.1 ± 0.05	-0.1 ± 0.05	37.6 ± 1.54	5250	1.10	-0.16	-

HD 41593	K0V	5300 ± 50	4.4 ± 0.05	0.1 ± 0.05	0.8 ± 0.05	5305	4.49	0.07	-
HD 50420	A9III	7200 ± 50	3.2 ± 0.05	0.0 ± 0.05	15.1 ± 0.39	7200	3.28	0.04	-
HD 60778	A1V	8400 ± 50	3.3 ± 0.05	-0.5 ± 0.05	3.7 ± 0.10	8416	3.30	-0.50	-
HD 61064	F6III	6400 ± 50	3.2 ± 0.05	0.4 ± 0.05	4.3 ± 0.05	6367	3.21	0.44	-
HD 63077	G0V	5700 ± 50	4.0 ± 0.05	-0.9 ± 0.05	1.3 ± 0.05	5731	4.08	-0.87	-
HD 65583	G8V	5300 ± 50	4.6 ± 0.05	-0.7 ± 0.05	0.8 ± 0.05	5295	4.64	-0.66	-
HD 67767	G8IV	5600 ± 50	4.4 ± 0.05	0.2 ± 0.05	2.7 ± 0.05	5598	4.37	0.17	-
HD 69897	F6V	6300 ± 50	4.2 ± 0.05	-0.3 ± 0.05	1.3 ± 0.05	6275	4.21	-0.31	1.3870 ± 0.0276[6]
HD 75732	G8V	5300 ± 50	4.3 ± 0.05	0.4 ± 0.05	0.9 ± 0.05	5256	4.38	0.37	0.960 ± 0.067 [24]
HD 76151	G3V	5800 ± 50	4.4 ± 0.05	0.1 ± 0.05	1.0 ± 0.05	5728	4.40	0.04	0.88[19]
HD 86728	G1V	5800 ± 50	4.3 ± 0.05	0.2 ± 0.05	1.3 ± 0.05	5737	4.25	0.12	1.247 ± 0.021[5]
HD 86986	A1V	7900 ± 50	3.1 ± 0.05	-1.7 ± 0.05	2.8 ± 0.07	7867	3.15	-1.77	-
HD 87737	A0Ib	9900 ± 50	2.0 ± 0.05	0.0 ± 0.05	27.8 ± 1.86	9806	1.95	-0.01	47[40]
HD 91316	B1Ib	24200 ± 50	3.1 ± 0.05	-0.8 ± 0.05	43.4 ± 13.02	24200	3.09	-0.89	-
HD 94028	F4V	6000 ± 50	4.2 ± 0.05	-1.5 ± 0.05	1.0 ± 0.05	5969	4.28	-1.45	-
HD 94247	K3III	4200 ± 50	2.2 ± 0.05	-0.1 ± 0.05	54.4 ± 1.18	4243	2.28	-0.16	-
HD 95418	A1V	9400 ± 50	4.0 ± 0.05	0.2 ± 0.05	3.4 ± 0.05	9452	3.94	0.22	-
HD 97633	A2V	9400 ± 50	3.6 ± 0.05	0.1 ± 0.05	3.9 ± 0.05	9360	3.60	0.03	-

HD 100006	K0III	4800 ± 50	3.0 ± 0.05	0.1 ± 0.05	11.6 ± 0.18	4755	3.00	0.02	-
HD 132142	K1V	5100 ± 50	4.5 ± 0.05	-0.6 ± 0.05	0.8 ± 0.05	5125	4.50	-0.55	-
HD 134083	F5V	6500 ± 50	4.2 ± 0.05	0.1 ± 0.05	1.4 ± 0.05	6583	4.20	0.06	-
HD 147394	B5IV	15000 ± 50	3.9 ± 0.05	-0.1 ± 0.05	3.9 ± 0.05	14908	3.81	-0.07	-
HD 164353	B5Ib	22200 ± 50	3.7 ± 0.05	-0.2 ± 0.05	17.3 ± 4.86	22150	3.73	-0.16	-

Table A.2: STELIB Dataset: Comparison of Parameter values from Kurucz Models (fit to only B band) with published values

A.1.3 Results for Fit over V-Band SED

Star	**Spectral Type**	Best Fit Parameter Values				Published Parameter Values			
		T_{eff} (K)	log(g) (dex)	[Fe/H] (dex)	$R/R_{\odot}$	T_{eff} (K)	log(g) (dex)	[Fe/H] (dex)	$R/R_{\odot}$
HD 2857	A2IV[30]	7600 ± 50	2.6 ± 0.05	-1.5 ± 0.05	4.2 ± 0.18	7611	2.67	-1.51	-
HD 32537	F0V	6900 ± 50	4.2 ± 0.05	-0.3 ± 0.05	2.1 ± 0.05	6978	4.07	-0.23	1.56[41]
HD 34411	G0V	5800 ± 50	4.1 ± 0.05	0.1 ± 0.05	1.3 ± 0.05	5845	4.13	0.01	1.331 ± 0.021[5]
HD 34816	B0.5IV	28700 ± 50	4.2 ± 0.05	-0.2 ± 0.05	4.8 ± 0.30	28724	4.20	-0.13	-
HD 35497	B7III	13400 ± 50	3.8 ± 0.05	-0.1 ± 0.05	5.0 ± 0.07	13429	3.80	-0.10	4.2[47]
HD 36673	F0Ib	7300 ± 50	1.4 ± 0.05	0.0 ± 0.05	171.2 ± 16.30	7276	1.31	-0.02	-
HD 37394	K1V	5100 ± 50	4.2 ± 0.05	-0.2 ± 0.05	1.3 ± 0.05	5194	4.12	-0.20	4.2[47]
HD 39949	G2Ib	5300 ± 50	1.1 ± 0.05	-0.1 ± 0.05	39.1 ± 1.60	5250	1.10	-0.16	-

HD 41593	K0V	5300 ± 50	4.5 ± 0.05	0.1 ± 0.05	0.8 ± 0.05	5305	4.49	0.07	-
HD 50420	A9III	7200 ± 50	3.3 ± 0.05	0.0 ± 0.05	15.0 ± 0.39	7200	3.28	0.04	-
HD 60778	A1V	8500 ± 50	3.3 ± 0.05	-0.5 ± 0.05	3.6 ± 0.10	8416	3.30	-0.50	-
HD 61064	F6III	6400 ± 50	3.2 ± 0.05	0.4 ± 0.05	4.4 ± 0.05	6367	3.21	0.44	-
HD 63077	G0V	5800 ± 50	4.0 ± 0.05	-0.9 ± 0.05	1.2 ± 0.05	5731	4.08	-0.87	-
HD 65583	G8V	5200 ± 50	4.6 ± 0.05	-0.7 ± 0.05	0.8 ± 0.05	5295	4.64	-0.66	-
HD 67767	G8IV	5500 ± 50	4.4 ± 0.05	0.1 ± 0.05	3.0 ± 0.05	5598	4.37	0.17	-
HD 69897	F6V	6200 ± 50	4.3 ± 0.05	-0.4 ± 0.05	1.4 ± 0.05	6275	4.21	-0.31	1.3870 ± 0.0276[6]
HD 75732	G8V	5300 ± 50	4.3 ± 0.05	0.4 ± 0.05	0.9 ± 0.05	5256	4.38	0.37	0.960 ± 0.067 [24]
HD 76151	G3V	5700 ± 50	4.4 ± 0.05	0.0 ± 0.05	1.1 ± 0.05	5728	4.40	0.04	0.88[19]
HD 86728	G1V	5800 ± 50	4.3 ± 0.05	0.1 ± 0.05	1.3 ± 0.05	5737	4.25	0.12	1.247 ± 0.021[5]
HD 86986	A1V	7900 ± 50	3.2 ± 0.05	-1.8 ± 0.05	2.9 ± 0.07	7867	3.15	-1.77	-
HD 87737	A0Ib	9800 ± 50	2.0 ± 0.05	0.0 ± 0.05	28.1 ± 1.86	9806	1.95	-0.01	47[40]
HD 91316	B1Ib	-	-	-	-	24200	3.09	-0.89	-
HD 94028	F4V	6000 ± 50	4.3 ± 0.05	-1.5 ± 0.05	1.0 ± 0.05	5969	4.28	-1.45	-
HD 94247	K3III	4300 ± 50	2.2 ± 0.05	-0.2 ± 0.05	48.7 ± 1.06	4243	2.28	-0.16	-
HD 95418	A1V	9500 ± 50	3.9 ± 0.05	0.3 ± 0.05	3.3 ± 0.05	9452	3.94	0.22	-
HD 97633	A2V	9400 ± 50	3.6 ± 0.05	0.1 ± 0.05	3.9 ± 0.05	9360	3.60	0.03	-

HD 100006	K0III	4700 ± 50	3.0 ± 0.05	0.0 ± 0.05	12.8 ± 0.19	4755	3.00	0.02	-
HD 132142	K1V	5100 ± 50	4.5 ± 0.05	-0.6 ± 0.05	0.9 ± 0.05	5125	4.50	-0.55	-
HD 134083	F5V	6600 ± 50	4.2 ± 0.05	0.1 ± 0.05	1.4 ± 0.05	6583	4.20	0.06	-
HD 147394	B5IV	14900 ± 50	3.8 ± 0.05	0.0 ± 0.05	4 ± 0.05	14908	3.81	-0.07	-
HD 164353	B5Ib	22100 ± 50	3.7 ± 0.05	-0.2 ± 0.05	17.0 ± 4.77	22150	3.73	-0.16	-

Table A.3: STELIB Dataset: Comparison of Parameter values from Kurucz Models (fit to only V band) with published values

A.1.4 Results for Synthetic Photometry over complete SED

Star	Synthetic photometry from spectra						Photoelectric photometry					
	U	B	V	R	I	M_v	U	B	V	R	I	M_v
HD 2857	10.01	9.91	9.76	9.66	9.79	$0.35^{+0.093}_{-0.01}$	10.42	10.19	9.99	-	-	-
HD 32537	4.7	4.79	4.42	4.21	4.08	$2.29^{+0.015}_{-0.01}$	-	-	-	4.8 [30]	-	$2.49^{+0.06}_{-0.06}$
HD 34411	5.33	5.28	4.59	4.25	3.99	$4.11^{+0.003}_{-0.01}$	5.45	5.33	4.71	4.18	3.86	$4.19^{+0.04}_{-0.04}$
HD 34816	3.05	4.05	4.3	4.39	4.94	$-2.79^{+0.14}_{-0.13}$	3.01	4.02	4.29	4.41	4.69	$-3.35^{+0.51}_{-0.65}$
HD 35497	0.91	1.41	1.51	1.54	1.7	$-1.55^{+0.03}_{-0.03}$	1.03	1.52	1.65	1.66	1.76	-
HD 36673	1.98	1.78	1.61	1.5	1.47	$-7.55^{+0.2}_{-0.2}$	3.04	2.79	2.58	2.36	2.15	$-6.11^{+0.56}_{-0.74}$
HD 37394	6.64	6.3	5.37	4.91	4.54	$4.92^{+0.001}_{-0.001}$	7.57	7.06	6.22	5.53	5.10	$5.07^{+0.04}_{-0.04}$
HD 39949	8.08	7.59	6.66	6.24	5.86	$-2.68^{+0.09}_{-0.09}$		8.32	7.23	-	-	-

HD 41593	7.97	7.64	6.73	6.3	5.96	$5.74^{+0.006}_{-0.004}$	8.016 [30]	7.565 [30]	-	6.2 [30]	-	$5.81^{+0.05}_{-0.05}$
HD 50420	5.58	5.51	5.2	5.03	4.89	$-2.17^{+0.05}_{-0.06}$	-	6.468 [30]	6.151 [30]	-	-	$-1.72^{+0.41}_{-0.50}$
HD 60778	8.9	8.82	8.74	8.68	8.72	$0.26^{+0.07}_{-0.06}$	9.44	9.22	9.11	-	-	-
HD 61064	5.74	5.6	5.02	4.74	4.54	$1.06^{+0.02}_{-0.02}$	5.67	5.57	5.13	-	-	$1.12^{+0.13}_{-0.14}$
HD 63077	5.81	5.98	5.37	5.03	4.9	$4.43^{+0.006}_{-0.004}$	5.87	5.94	5.36	-	-	$4.46^{+0.04}_{-0.04}$
HD 65583	8.04	7.9	7.04	6.61	6.39	$5.87^{+0.007}_{-0.003}$	7.89	7.71	7.00	6.40	5.98	$5.87^{+0.05}_{-0.05}$
HD 67767	6.74	6.55	5.74	5.35	5.22	$2.71^{+0.01}_{-0.01}$	6.98	6.54	5.72	5.41	5.14	$2.61^{+0.08}_{-0.09}$
HD 69897	5.53	5.66	5.13	4.84	4.57	$3.82^{+0.007}_{-0.003}$	5.54	5.60	5.14	-	-	$3.82^{+0.05}_{-0.05}$
HD 75732	7.35	6.85	5.86	5.4	5.2	$5.36^{+0.005}_{-0.005}$	7.46	6.81	5.95	5.66	5.40	$5.46^{+0.04}_{-0.04}$
HD 76151	6.71	6.63	5.9	5.55	5.27	$4.77^{+0.001}_{-0.001}$	6.88	6.66	6.00	5.64	5.31	$4.74^{+0.05}_{-0.05}$
HD 86728	5.91	5.8	5.06	4.7	4.6	$4.19^{+0.008}_{-0.002}$	6.28	6.02	5.37	4.9 [30]	-	$4.32^{+0.04}_{-0.04}$
HD 86986	8.6	8.52	8.33	8.27	8.44	$1.07^{+0.05}_{-0.05}$	8.27 [30]	8.11 [30]	-	7.9 [30]	-	$0.54^{+0.51}_{-0.65}$
HD 87737	2.99	3.23	3.25	3.23	3.52	$-4.7^{+0.138}_{-0.13}$	3.25	3.46	3.49	3.40	3.38	-
HD 91316	2.62	3.59	3.53	3.43	4.32	$-7.58^{+0.78}_{-0.57}$	2.76	3.71	3.85	3.89	4.05	-
HD 94028	8.45	8.73	8.2	7.89	7.79	$4.71^{+0.01}_{-0.01}$	8.52	8.70	8.23	7.76	7.46	$4.63^{+0.15}_{-0.16}$
HD 94247	6.73	5.75	4.43	3.82	3.36	$-1.76^{+0.04}_{-0.05}$	7.97	6.45	5.09	4.49	4.00	$-2.16^{+0.28}_{-0.32}$
HD 95418	2.08	2.11	2.07	2.06	2.36	$0.13^{+0.006}_{-0.005}$	2.35	2.35	2.37	2.31	2.35	-
HD 97633	3.28	3.32	3.31	3.29	3.59	$-0.21^{+0.02}_{-0.02}$	3.37	3.33	3.34	3.35	3.35	$-0.38^{+0.11}_{-0.11}$

HD 100006	7.32	6.65	5.52	5.01	4.71	$0.44^{+0.04}_{-0.03}$	7.41	6.59	5.53	5.04	4.68	$0.56^{+0.20}_{-0.22}$
HD 132142	8.74	8.49	7.59	7.14	6.72	$5.73^{+0.004}_{-0.01}$	8.90	8.56	7.78	7.11	6.66	$5.87^{+0.05}_{-0.05}$
HD 134083	5.26	5.33	4.84	4.58	4.6	$3.41^{+0.005}_{-0.01}$	5.33	5.36	4.93	4.53	4.32	$3.45^{+0.05}_{-0.05}$
HD 147394	2.96	3.54	3.66	3.7	4.13	$-1.21^{+0.03}_{-0.02}$	3.19	3.75	3.90	3.98	4.14	$-1.13^{+0.13}_{-0.13}$
HD 164353	2.57	3.47	3.67	3.74	4.25	$-5.1^{+0.7}_{-0.5}$	3.34	3.99	3.97	3.91	3.88	-

Table A.4: STELIB Dataset: Comparison of Synthetic Photometry of spectra from Kurucz Models with published values (from SIMBAD database and J.-F. Le Borgne et al., (2003))

A.1.5 Results for Synthetic Photometry over only B and only V band SED separately

Star	Synthetic photometry			Photoelectric photometry		
	B	V	M_v	B	V	M_v
HD 2857	9.84	9.81	$0.39^{+0.1}_{-0.1}$	10.19	9.99	-
HD 32537	4.83	4.48	$2.34^{+0.001}_{-0.001}$	-	-	$2.49^{+0.06}_{-0.06}$
HD 34411	5.35	4.68	$4.2^{+0.005}_{-0.01}$	5.33	4.71	$4.19^{+0.04}_{-0.04}$
HD 34816	4.02	4.27	$-2.81^{+0.14}_{-0.14}$	4.02	4.29	$-3.35^{+0.51}_{-0.65}$
HD 35497	1.41	1.57	$-1.5^{+0.03}_{-0.03}$	1.52	1.65	-
HD 36673	1.81	1.6	$-7.56^{+0.2}_{-0.2}$	2.79	2.58	$-6.11^{+0.56}_{-0.74}$
HD 37394	6.25	5.37	$4.92^{+0.005}_{-0.004}$	7.06	6.22	$5.07^{+0.04}_{-0.04}$
HD 39949	7.75	6.61	$-2.73^{+0.09}_{-0.09}$	8.32	7.23	-

HD 41593	7.58	6.74	$5.75^{+0.001}_{-0.003}$	7.565 [30]	-	$5.81^{+0.05}_{-0.05}$
HD 50420	5.46	5.2	$-2.17^{+0.05}_{-0.06}$	6.468 [30]	6.151 [30]	$-1.72^{+0.41}_{-0.50}$
HD 60778	8.84	8.76	$0.28^{+0.07}_{-0.06}$	9.22	9.11	-
HD 61064	5.55	4.99	$1.02^{+0.02}_{-0.02}$	5.57	5.13	$1.12^{+0.13}_{-0.14}$
HD 63077	5.89	5.37	$4.44^{+0.004}_{-0.012}$	5.94	5.36	$4.46^{+0.04}_{-0.04}$
HD 65583	7.7	7.04	$5.88^{+0.004}_{-0.005}$	7.71	7.00	$5.87^{+0.05}_{-0.05}$
HD 67767	6.57	5.7	$2.67^{+0.01}_{-0.01}$	6.54	5.72	$2.61^{+0.08}_{-0.09}$
HD 69897	5.62	5.05	$3.75^{+0.01}_{-0.01}$	5.60	5.14	$3.82^{+0.05}_{-0.05}$
HD 75732	6.87	5.98	$5.48^{+0.005}_{-0.005}$	6.81	5.95	$5.46^{+0.04}_{-0.04}$
HD 76151	6.58	5.79	$4.66^{+0.001}_{-0.001}$	6.66	6.00	$4.74^{+0.05}_{-0.05}$
HD 86728	5.75	5.07	$4.2^{+0.008}_{-0.005}$	6.02	5.37	$4.32^{+0.04}_{-0.04}$
HD 86986	8.48	8.6	$1.34^{+0.05}_{-0.05}$	8.11 [30]	-	$0.54^{+0.51}_{-0.65}$
HD 87737	3.34	3.38	$-4.57^{+0.14}_{-0.14}$	3.46	3.49	-
HD 91316	3.62	-	-	3.71	3.85	-
HD 94028	8.71	8.2	$4.71^{+0.01}_{-0.01}$	8.70	8.23	$4.63^{+0.15}_{-0.16}$
HD 94247	5.68	4.4	$-1.79^{+0.04}_{-0.05}$	6.45	5.09	$-2.16^{+0.28}_{-0.32}$
HD 95418	2.02	2.05	$0.11^{+0.01}_{-0.01}$	2.35	2.37	-
HD 97633	3.29	3.31	$-0.21^{+0.02}_{-0.02}$	3.33	3.34	$-0.38^{+0.11}_{-0.11}$

HD 100006	6.68	5.55	$0.47^{+0.03}_{-0.034}$	6.59	5.53	$0.56^{+0.20}_{-0.22}$
HD 132142	8.68	7.59	$5.73^{+0.001}_{-0.001}$	8.56	7.78	$5.87^{+0.05}_{-0.05}$
HD 134083	5.39	4.84	$3.41^{+0.012}_{-0.01}$	5.36	4.93	$3.45^{+0.05}_{-0.05}$
HD 147394	3.57	3.66	$-1.21^{+0.023}_{-0.025}$	3.75	3.90	$-1.13^{+0.13}_{-0.13}$
HD 164353	3.45	3.7	$-5.06^{+0.72}_{-0.54}$	3.99	3.97	-

Table A.5: STELIB Dataset: Comparison of Synthetic Photometry of spectra from Kurucz Models (B and V band only) with published values (from SIMBAD database and J.-F. Le Borgne et al., (2003))

A.2 IRTF Dataset Results

Star	**Spectral Type**	Best Fit Parameter Values				Published Parameter Values			
		T_{eff} (K)	log(g) (dex)	[Fe/H] (dex)	$R/R_{\odot}$	T_{eff} (K)	log(g) (dex)	[Fe/H] (dex)	$R/R_{\odot}$
HD 10476	K1V	5200 ± 50	4.5 ± 0.05	-0.1 ± 0.05	0.8 ± 0.05	5242± 3.2[23]	4.50 [17]	-0.04 [18]	0.80 ± 0.06 [36]
HD 11443	F6IV	6200 ± 50	3.9 ± 0.05	-0.1 ± 0.05	3.2 ± 0.05	6288 [4]	3.91 [4]	-0.09 [33]	3.22 [14]
HD 21770	G4III	6700 ± 50	3.9 ± 0.05	-0.2 ± 0.05	2.2 ± 0.05	6546^{126}_{176} [7]	3.94 [10]	-0.17 [10]	$2.28^{+0.13}_{-0.09}$ [7]
HD 25975	K1III	5000 ± 50	3.4 ± 0.05	0.1 ± 0.05	3.6 ± 0.05	5028^{+61}_{-70} [7]	3.45 [25]	0.02 ± 0.04[3]	$3.72^{+0.10}_{-0.09}$ [7]
HD 74395	G1Ib	5300 ± 50	2.0 ± 0.05	0.0 ± 0.05	32.2 ± 2.05	5370 [26]	2.08 [26]	-0.01 [22]	110 [35]
HD 100006	K0III	4700 ± 50	3.0 ± 0.05	0.0 ± 0.05	11.9 ± 0.18	4755[21]	3.00[21]	0.02[21]	-[21]
HD 101501	G8V	5300 ± 50	4.6 ± 0.05	0.1 ± 0.05	0.9 ± 0.05	5270 ± 32 [5]	4.69 [13]	0.03[13]	0.940 ± 0.010[5]

HD 102870	F8.5 IV-V	6100 ± 50	4.2 ± 0.05	0.2 ± 0.05	1.7 ± 0.05	6132 ± 26 [5]	4.25 [15]	0.20[15]	1.681 ± 0.008[5]
HD 114710	F9.5V	6200 ± 50	3.9 ± 0.05	0.1 ± 0.05	1.1 ± 0.05	5936 ± 33 [5]	4.38 [28]	0.07[28]	1.106 ± 0.011[5]
HD 115617	G6.5V	5600 ± 50	4.5 ± 0.05	0.0 ± 0.05	1.0 ± 0.05	5538 ± 13[49]	4.5 [37]	-0.02 [37]	0.9867± 0.0048[49]
HD 120477	K5.5III	3900 ± 50	1.5 ± 0.05	-0.2 ± 0.05	0.8 ± 0.05	3920 [44]	1.5 [31]	-0.23 [31]	38.44 ± 2.37[38]
HD 124850	F7III	6200 ± 50	4.0 ± 0.05	-0.2 ± 0.05	2.6 ± 0.05	6282[29]	3.94 [29]	-0.11 [29]	2.5[27]
HD 126660	F7V	6200 ± 50	4.1 ± 0.05	0.1 ± 0.05	1.7 ± 0.05	6265 ± 41[5]	4.12 [27]	0.02[39]	1.733± 0.011[5]
HD 142091	K1IVa	4900 ± 50	3.0 ± 0.05	0.2 ± 0.05	4.8 ± 0.05	4876 ± 46[50]	3.15± 0.14[50]	0.13 ± 0.03[50]	4.77 ± 0.07 [50]
HD 220657	F8III	5800 ± 50	3.3 ± 0.05	-0.1 ± 0.05	5.7 ± 0.05	6061^{+97}_{-178} [7]	3.22 [2]	-0.01 [3]	$5.97^{+0.36}_{-0.19}$ [7]

Table A.6: IRTF Dataset: Comparison of Parameter values from Kurucz Models with published values

Star	From Kurucz Models			From 2MASS		
	J	H	Ks	J	H	Ks
HD 10476	3.81	3.85	3.31	3.855±0.240	3.391±0.226	3.285±0.266
HD 11443	2.41	2.13	2.12	2.406±0.236	2.182±0.206	2.274±0.266
HD 21770	4.47	4.26	4.25	4.696±0.240	4.442±0.194	4.241±0.036
HD 25975	4.52	4.02	3.97	4.599±0.304	4.057±0.246	4.022±0.366
HD 74395	3.18	2.77	2.72	3.194±0.278	2.786±0.262	2.710±0.300
HD 100006	3.91	3.33	3.25	3.970±0.266	3.379±0.216	3.122±0.330
HD 101501	4.0	3.56	3.53	3.988±0.242	3.648±0.228	3.588±0.036
HD 102870	2.55	2.27	2.26	2.597±0.252	2.363±0.230	2.269±0.254
HD 114710	3.19	2.87	2.85	3.232±0.234	2.992±0.192	2.923±0.274
HD 115617	3.39	3.01	2.98	3.334±0.200	2.974±0.176	2.956±0.236
HD 120477	1.31	0.45	0.31	1.218±0.264	0.438±0.180	0.435±0.182
HD 124850	3.16	2.88	2.87	3.140±0.266	2.909±0.236	2.801±0.266
HD 126660	3.14	2.87	2.86	3.179±0.244	2.980±0.216	2.739±0.332
HD 142091	3.06	2.55	2.49	3.035±0.184	2.575±0.180	2.423±0.242
HD 220657	3.46	3.12	3.1	3.527±0.266	3.230±0.208	3.033±0.256

Table A.7: IRTF Dataset: Comparison of Synthetic Photometry of spectra from Kurucz Models with published values)

Bibliography

[1] *Allard et al. 1998, A&A, 335,1124*

[2] *Allende Prieto, C.; Lambert, D. L. (1999). "Fundamental parameters of nearby stars from the comparison with evolutionary calculations: Masses, radii and effective temperatures". Astronomy and Astrophysics. 352: 555. arXiv:astro-ph/9911002. Bibcode:1999A&A...352..555A. Vizier catalog entry*

[3] *Anderson, E.; Francis, Ch. (2012). "XHIP: An extended hipparcos compilation". Astronomy Letters. 38 (5): 331. arXiv:1108.4971. Bibcode:2012AstL...38..331A. doi:10.1134/S1063773712050015. Vizier catalog entry*

[4] *Balachandran, Suchitra (May 1990), "Lithium depletion and rotation in main-sequence stars", Astrophysical Journal, Part 1, 354: 310–332, Bibcode:1990ApJ...354..310B, doi:10.1086/168691*

[5] *Boyajian, Tabetha S.; et al. (February 2012), "Stellar Diameters and Temperatures. I. Main-sequence A, F, and G Stars", The Astrophysical Journal, 746 (1): 101, arXiv:1112.3316, Bibcode:2012ApJ...746..101B, doi:10.1088/0004-637X/746/1/101.. See Table 10.*

[6] *Boyajian, Tabetha S.; et al. (July 2013), "Stellar Diameters and Temperatures. III. Main-sequence A, F, G, and K Stars: Additional High-precision Measurements and Empirical Relations", The Astrophysical Journal, 771 (1): 40, arXiv:1306.2974, Bibcode:2013ApJ...771...40B, doi:10.1088/0004-637X/771/1/40.*

[7] *Brown, A. G. A.; et al. (Gaia collaboration) (August 2018). "Gaia Data Release 2: Summary of the contents and survey properties". Astronomy &*

Astrophysics. 616. A1. arXiv:1804.09365. Bibcode:2018A&A...616A...1G. doi:10.1051/0004-6361/201833051. Gaia DR2 record for this source at VizieR.

[8] *Carnall A. C., SpectRes: A Fast Spectral Resampling Tool in Python, arXiv:1705.05165, 2017*

[9]

[10] *Casagrande, L.; et al. (June 2011). "New constraints on the chemical evolution of the solar neighbourhood and Galactic disc(s). Improved astrophysical parameters for the Geneva-Copenhagen Survey". Astronomy and Astrophysics. 530: A138. arXiv:1103.4651. Bibcode:2011A&A...530A.138C. doi:10.1051/0004-6361/201016276. Castelli F. and Munari U., High resolution spectroscopy over 8500-8750Å for GAIA III. A library of synthetic spectra for 7750≤Te≤50000 K, A&A 366, 1003-1007 (2001), DOI: 10.1051/0004-6361:20000331*

[11] *Castelli F., Kurucz R.L., New Grids of ATLAS9 Model Atmospheres, IAU Symp. No 210, Modelling of Stellar Atmospheres, eds. N. Piskunov et al. 2003, poster A20, arXiv:astro-ph/0405087 (2004)*

[12] *Chavez M., Malagnini M.L., and Morossi C., An Atlas of high resolution synthetic spectra in the wavelength region 4850-5400Å, Astronomy and Astrophysics Supplement Series 126,267-272 (1997)*

[13] *Cornide, M.; Rego, M. (October 1984). "Iron abundances in G dwarfs". Astrophysics and Space Science. 105 (1): 55–65. Bibcode:1984Ap&SS.105...55C. doi:10.1007/BF00651207.*

[14] *Fuhrmann, Klaus (February 2008), "Nearby stars of the Galactic disc and halo - IV", Monthly Notices of the Royal Astronomical Society, 384 (1): 173–224, Bibcode:2008MNRAS.384..173F, doi:10.1111/j.1365-2966.2007.12671.x*

[15] *Gehren, T. (1978). "On the chemical composition and age of Beta VIR". Astronomy and Astrophysics. 65 (3): 427–433. Bibcode:1978A&A....65..427G.*

[16] *George B. Rybicki and Alan P. Lightman, "Radiative Processes in Astrophysics*

[17] *HD 10476, catalog entry, Fundamental parameters and elemental abundances of 160 F-G-K stars based on OAO spectrum database, Y. Takeda, CDS ID J/PASJ/59/335; see also Publications of the Astronomical Society of Japan 59, #2 (April 2007), pp. 335–356, Bibcode: 2007PASJ...59..335T.*

[18] *HD 10476, database entry, The Geneva-Copenhagen Survey of Solar neighbourhood, J. Holmberg et al., 2007, CDS ID V/117A. Accessed on line November 19, 2008.*

[19] *HD 76151, database entry, Catalog of Apparent Diameters and Absolute Radii of Stars (CADARS), 3rd edition, L. E. Pasinetti-Fracassini, L. Pastori, S. Covino, and A. Pozzi, CDS ID II/224. Accessed on line January 20, 2011.*

[20] *Huchra, John. "Astronomical Magnitude Systems". Harvard-Smithsonian Center for Astrophysics. Archived from the original on 21 July 2018. Retrieved 18 July 2017.*

[21] *J.-F. Le Borgne, et al. "STELIB: a library of stellar spectra at R 2000", Astron.Astrophys.402:433-442,2003, arXiv:astro-ph/0302334, doi: 10.1051/0004-6361:20030243.*

[22] *Kovtyukh, V. V.; Gorlova, N. I.; Belik, S. I. (2012). "Accurate luminosities from the oxygen λ7771-4 Å triplet and the fundamental parameters of F-G supergiants". Monthly Notices of the Royal Astronomical Society. 423 (4): 3268. arXiv:1204.4115. Bibcode:2012MNRAS.423.3268K. doi:10.1111/j.1365-2966.2012.21117.x.*

[23] *Kovtyukh; Soubiran, C.; Belik, S. I.; Gorlova, N. I. (2003), "High precision effective temperatures for 181 F-K dwarfs from line-depth ratios", Astronomy and Astrophysics, 411 (3): 559–564, arXiv:astro-ph/0308429, Bibcode:2003A&A...411..559K, doi:10.1051/0004-6361:20031378.*

[24] *Ligi, R.; et al. (February 2016), "Radii, masses, and ages of 18 bright stars using interferometry and new estimations of exoplanetary parameters", Astronomy & Astrophysics, 586: 23, arXiv:1511.03197, Bibcode:2016A&A...586A..94L, doi:10.1051/0004-6361/201527054, A94.*

[25] *Luck, R. Earle (January 2017), "Abundances in the Local Region II: F, G, and K Dwarfs and Subgiants", The Astronomical Journal, 153 (1):*

19, arXiv:1611.02897, Bibcode:2017AJ....153...21L, doi:10.3847/1538-3881/153/1/21, 21.

[26] *Lyubimkov, Leonid S.; Lambert, David L.; Korotin, Sergey A.; Rachkovskaya, Tamara M.; Poklad, Dmitry B. (2015). "Carbon abundance and the N/C ratio in atmospheres of A-, F- and G-type supergiants and bright giants". Monthly Notices of the Royal Astronomical Society. 446 (4): 3447. arXiv:1411.2722. Bibcode:2015MNRAS.446.3447L. doi:10.1093/mnras/stu2299.*

[27] *Malagnini, M. L.; Morossi, C. (November 1990). "Accurate absolute luminosities, effective temperatures, radii, masses and surface gravities for a selected sample of field stars". Astronomy and Astrophysics Supplement Series. 85 (3): 1015–1019. Bibcode:1990A&AS...85.1015M.*

[28] *Mallik, Sushma V. (October 1998). "Chromospheric activity in cool stars and the lithium abundance". Astronomy and Astrophysics. 338: 623–636. Bibcode:1998A&A...338..623M.*

[29] *Mallik, Sushma V. (December 1999). "Lithium abundance and mass". Astronomy and Astrophysics. 352: 495–507. Bibcode:1999A&A...352..495M.*

[30] *Marc Wenger et al., (2000). "The SIMBAD Astonomical Database", arXiv:astro-ph/0002110, doi: 10.1051/aas:2000332*

[31] *Massarotti, Alessandro; et al. (January 2008), "Rotational and Radial Velocities for a Sample of 761 HIPPARCOS Giants and the Role of Binarity", The Astronomical Journal, 135 (1): 209–231, Bibcode:2008AJ....135..209M, doi:10.1088/0004-6256/135/1/209.*

[32] *Murphy T. and Meiksin A., A library of high-resolution Kurucz spectra in the range λλ3000-10000, Mon. Not. R. Astron. Soc. 351, 1430-1438 (2004), doi:10.1111/j.1365-2966.2004.07895.x*

[33] *Nordström, B.; et al. (May 2004), "The Geneva-Copenhagen survey of the Solar neighbourhood. Ages, metallicities, and kinematic properties of ˜14 000 F and G dwarfs", Astronomy and Astrophysics, 418: 989–1019, arXiv:astro-ph/0405198, Bibcode:2004A&A...418..989N, doi:10.1051/0004-6361:20035959*

[34] *Partridge & Schwenke 1997, J. Chem. Phys., 106, 4618*

[35] *Pasinetti Fracassini, L. E.; Pastori, L.; Covino, S.; Pozzi, A. (2001). "Catalogue of Apparent Diameters and Absolute Radii of Stars (CADARS) - Third edition - Comments and statistics". Astronomy and Astrophysics. 367 (2): 521. arXiv:astro-ph/0012289. Bibcode:2001A&A...367..521P. doi:10.1051/0004-6361:20000451.*

[36] *Perrin, M.-N. (1987), "Stellar radius determination from IRAS 12-micron fluxes", Astronomy and Astrophysics, 172: 235-240, Bibcode:1987A&A...172..235P.*

[37] *Perrin, M.-N.; Cayrel de Strobel, G.; Dennefeld, M. (February 1988), "High S/N detailed spectral analysis of four G and K dwarfs within 10 PC of the sun", Astronomy and Astrophysics, 191 (2): 237–247, Bibcode:1988A&A...191..237P*

[38] *Piau, L.; et al. (2010), "Surface convection and red giants radii measurements", Astronomy and Astrophysics, 526: 12, arXiv:1010.3649, Bibcode:2011A&A...526A.100P, doi:10.1051/0004-6361/201014442, A100.*

[39] *Prugniel, P.; Vauglin, I.; Koleva, M. (2011). "The atmospheric parameters and spectral interpolator for the MILES stars". Astronomy & Astrophysics. 531: A165. arXiv:1104.4952. Bibcode:2011A&A...531A.165P. doi:10.1051/0004-6361/201116769.*

[40] *Przybilla, N.; Butler, K.; Becker, S. R.; Kudritzki, R. P. (2006). "Quantitative spectroscopy of BA-type supergiants". Astronomy and Astrophysics. 445 (3): 1099. arXiv:astro-ph/0509669. Bibcode:2006A&A...445.1099P. doi:10.1051/0004-6361:20053832.*

[41] *Rachford, Brian L.; Foight, Dillon R. (2009). "Chromospheric Variability in Early F-Type Stars". The Astrophysical Journal. 698: 786. arXiv:0904.1620. Bibcode:2009ApJ...698..786R. doi:10.1088/0004-637X/698/1/786.*

[42] *Rayner J.T., et al. SpeX: A Medium-Resolution 0.8–5.5 Micron Spectrograph and Imager for the NASA Infrared Telescope Facility, Publications of the Astronomical Society of the Pacific, 115:362–382, 2003 March*

[43] *Rosaria Tantalo, Cesare Chiosi, Measuring age, metallicity and abundance ratios from absorption-line indices, MNRAS, Volume 353, Issue 3, September 2004, Pages 917–940, https://doi.org/10.1111/j.1365-2966.2004.08123.x*

[44] *Stello, D.; et al. (2008), "Oscillating K Giants with the WIRE Satellite: Determination of Their Asteroseismic Masses", The Astrophysical Journal Letters, 674 (1): L53–L56, arXiv:0801.2155, Bibcode:2008ApJ...674L..53S, doi:10.1086/528936.*

[45] *Straizys V., Liubertas R. and Valiauga G., Kurucz Model FLux Distributions: A Comparison With Real Stars, Baltic Astronomy, vol. 6, 601-636, 1997.*

[46] *Straizys V., Liubertas R. and Valiauga G., Kurucz Model FLux Distributions: A Comparison With Real Stars. II Metal-Deficient Stars, Baltic Astronomy, vol. 11, 341-366, 2002.*

[47] *Underhill, A. B.; et al. (November 1979), "Effective temperatures, angular diameters, distances and linear radii for 160 O and B stars", Monthly Notices of the Royal Astronomical Society, 189 (3): 601–605, Bibcode:1979MNRAS.189..601U, doi:10.1093/mnras/189.3.601*

[48] *Valenti J.A. and Piskunov N., Spectroscopy made easy: A new tool for fitting observations with synthetic spectra, Astron. Astrophys. Suppl. Ser.118,595-603 (1996)*

[49] *von Braun, Kaspar; et al. (2014). "Stellar diameters and temperatures - V. 11 newly characterized exoplanet host stars". Monthly Notices of the Royal Astronomical Society. 438 (3): 2413–2425. arXiv:1312.1792. Bibcode:2014MNRAS.438.2413V. doi:10.1093/mnras/stt2360.*

[50] *White, T. R.; et al. (July 2018). "Interferometric diameters of five evolved intermediate-mass planet-hosting stars measured with PAVO at the CHARA Array". Monthly Notices of the Royal Astronomical Society. 477 (4): 4403–4413. arXiv:1804.05976. Bibcode:2018MNRAS.477.4403W. doi:10.1093/mnras/sty898.*

[51] *http://svo2.cab.inta-csic.es/theory/fps/index.php?mode=browse&gname=2MASS&ftypes=*

[52] *http://kurucz.harvard.edu/papers/sao309/*

[53] *https://www.stsci.edu/hst/instrumentation/reference-data-for-calibration-and-tools/astronomical-catalogs/castelli-and-kurucz-atlas*

[54] *https://pysynphot.readthedocs.io/en/latest/*

[55] *http://irtfweb.ifa.hawaii.edu/∼spex/IRTF_Spectral_Library/References_files/All.html*

[56] *https://www.aip.de/en/research/facilities/stella/instruments/data/johnson-ubvri-filter-curves*

[57] *http://cosmos.astro.caltech.edu/page/filterset*

[58] *https://en.wikipedia.org/wiki/Astronomical_spectroscopy*